CZECH TECHNICAL UNIVERSITY IN PRAGUE

FACULTY OF ELECTRICAL ENGINEERING

Spectral Response of Photovoltaic Cells and Modules

MASTER THESIS

Bc. Sándor Ádám

2021

Supervisor: Ing. Ladislava Černá, Ph.D.

ZADÁNÍ DIPLOMOVÉ PRÁCE

I. OSOBNÍ A STUDIJNÍ ÚDAJE

Příjmení: **Ádám** Jméno: **Sándor** Osobní číslo: **469846**

Fakulta/ústav: **Fakulta elektrotechnická**

Zadávající katedra/ústav: **Katedra elektrotechnologie**

Studijní program: **Elektrotechnika, energetika a management**

Specializace: **Technologické systémy**

II. ÚDAJE K DIPLOMOVÉ PRÁCI

Název diplomové práce:

Spektrální odezva fotovoltaických článků a modulů

Název diplomové práce anglicky:

Spectral Response of Photovoltaic Cells and Modules

Pokyny pro vypracování:

1) Změřte spektrální odezvu fotovoltaických článků různého typu s využitím laserů.
2) Pokuste se změřit s využitím laserů spektrální odezvu jednoho článku v rámci modulu.
3) Vyhodnoťte homogenitu spektrální odezvy.
4) Navrhněte metodiku přepočtu spektrální citlivosti z naměřených údajů na spektrum AM1.5.

Seznam doporučené literatury:

[1] LUQUE, A., HEGEDUS, S. Handbook of photovoltaic science and engineering [online]. 2. Hoboken, NJ: Wiley, c2011. ISBN 978-0-470-97466-7. Available at: http://eu.wiley.com/WileyCDA/WileyTitle/productCd-0470976128.html

Jméno a pracoviště vedoucí(ho) diplomové práce:

Ing. Ladislava Černá, Ph.D., katedra elektrotechnologie FEL

Jméno a pracoviště druhé(ho) vedoucí(ho) nebo konzultanta(ky) diplomové práce:

Datum zadání diplomové práce: **22.01.2021** Termín odevzdání diplomové práce: **13.08.2021**

Platnost zadání diplomové práce: **30.09.2022**

Ing. Ladislava Černá, Ph.D. podpis vedoucí(ho) práce	podpis vedoucí(ho) ústavu/katedry	prof. Mgr. Petr Páta, Ph.D. podpis děkana(ky)

III. PŘEVZETÍ ZADÁNÍ

Diplomant bere na vědomí, že je povinen vypracovat diplomovou práci samostatně, bez cizí pomoci, s výjimkou poskytnutých konzultací. Seznam použité literatury, jiných pramenů a jmen konzultantů je třeba uvést v diplomové práci.

Datum převzetí zadání	Podpis studenta

Prohlášení

Prohlašuji, že jsem předloženou práci vypracoval samostatně a že jsem uvedl veškeré použité informační zdroje v souladu s Metodickým pokynem o dodržování etických principů při přípravě vysokoškolských závěrečných prací.

V Praze dne 13.8.2021

Sándor Ádám

Acknowledgments

I would like to thank my supervisor Ing. Ladislava Černá, PhD. for the great support I got from her, also for her technical advice, patience, and comments regarding the work. I am also thankful to my supervisors from the Polytechnic University of Valencia, Spain, to prof. Prof. Dr. Bernabé Marí and Prof. Dr. Salvador Seguí-Chilet for their coordination and help in the experimental part of this work. Last but not least, I am deeply thankful to my family for supporting me during the years of my study.

Anotace

Táto práca sa zabýva so spektrálnou odozvou fotovoltaických článkov a modulov. Je zameraná najmä na teoretický popis fotovoltaických článkov, princíp fungovania a na experimenty na určenie spektrálnej odozvy a homogenity spektrálnej odozvy. Ďalej na dôležité aspekty spektrálnej odozvy fotovoltaických jednotlivých článkov v rámci modulu.

Klíčová slova

spektrálna odozva, fotovoltaické články, AM 1.5, homogenita spektrálnej odozvy

Annotation

This work deals with the spectral response of photovoltaic cells and modules. It focuses mainly on the theoretical description of PV cells and on experiments to determine the spectral response and homogeneity of the spectral response. Furthermore, essential aspects of the spectral response of photovoltaic cells within a module.

Key words

spectral response, photovoltaic cells, AM 1.5, homogeneity of spectral response

CONTENTS

INTRODUCTION

Photovoltaic technology is one of the most important part of our everyday life even if we are not aware of it. It plays a huge role not just in giving us the ability to power our everyday life but doing all this in a sustanaible and ecologicall way. It can have a big impact in developing regions of the world as we are headed to an uncertain world with regard to climate change.

Energy from the sun on the Earth represents almost all sources of the energies. Plant matter which was created by biological processes were fueled by the energy of the Sun itself. Also fossil fuels which are present on the earth just represent the energy from the Sun cumulated from billions and millions of years ago.

Also biological sources of energy like biomass come from solar energy. This energy can be used for producing electricity, heating homes and in the transportation as well. Wind energy based on the Earth's rotation and air currents that were created by the Suns ability to heat up the air has been used to create mechanical energy or transport things. Today we utilize this energy by wind turbines in converting wind power to electricity. With photovoltaics, there is an elegant and easy method of using solar energy. PV plants are unique in that they directly convert incident sunlight into electricity without noise making them a reliable and long-lasting solution without major pollution.

Another topic of discussion is the effectiveness of these PV modules and cells. This parameter is greatly influenced by many factors, which of course depend not only on the properties of the materials used but also on the location and ambient temperature. These parameters can be examined mainly experimentally in various ways.

In this work we will deal with these possibilities and for that our focus will be on the spectral analysis of photovoltaic cells and modules. We will examine the different types of solar cells as well as their properties, advantages, disadvantages. Later with experiments based on previous studies we determine their spectral response, quantum efficiency for the whole module as well as for a cell within a module. Evaulation of homogeinity of these different types of cells is also a big focus of this work. New materials still in development are also tested as this can get us helpful data in comparing them with technologies which are in use already. With determining these parameters we can get a broader picture of what type of work lays still aheod with regard to optimizing the performance of these cells.

1. PROPERTIES OF LIGHT

Light or visible light is electromagnetic radiation in the electromagnetic spectrum that the human eye can perceive.

The scientific description of light as a wave first became known in the early 19th century by Thomas Young, François Arag and Augustine Jean Fresnel when they showed interference effects in light rays, pointing at the direction that light is formed by waves. The electromagnetic spectrum describes light as a wave that has a specific wavelength. In the late 1960s, light was considered part of the electromagnetic spectrum. At the end of nineteen years, however, a problem with the wavelength view of light emerged when the wave equations of light could not explain experiments measuring the wavelength spectrum from heated objects. This discrepancy has been solved. Planck suggested that the total energy of light consists of unrecognizable energy elements or an amount of energy. In investigating the photoelectric effect (the release of electrons from certain metals and semiconductors under the impact of light), Einstein correctly distinguished the values of these elements of quantum energy. Max Planck and Albert Einstein won the Nobel Prize in Physics in 1918 and 1921 for their work in this field, and based on the work, light can be seen as consisting of packets called photons. [1]

Nowadays quantum mechanics can explain the observations of the wave nature as well as the particle nature of light. In modern quantum mechanics, a photon, like all other quantum-mechanical particles such as electrons, protons, etc., is most accurately represented as a wave packet. A wave packet is defined as a set of waves that can interact so that a wave packet can either appear spatially localized or can alternately appear simply as a wave. In cases where the wave packet is spatially localized, it acts as a particle. Therefore, depending on the situation, the photon may appear as a wave or as a particle, and this concept is called wave-particle duality. [1]

The photon is characterized either by the wavelength denoted by λ, or equivalent by the energy represented by E. We can write an inverse between the photon energy (E) and the wavelength of light (λ) given by the equation:

$$E = \frac{hc}{\lambda}$$

where h is the Planck constant and c is the speed of light. [2]

A complete physical description of light properties requires in-depth quantum-mechanical analysis of light. This level of detail is rarely needed for photovoltaic applications. However, in some situations, light can behave in a way contrary to common sense.

1.1. Electromagnetic spectrum

The electromagnetic spectrum describes the wide range of frequencies of electromagnetic radiation and their wavelengths and energies of the photons.

The electromagnetic spectrum covers electromagnetic waves with frequencies from 1 Hz to 1025 Hz, which corresponds to wavelengths from thousands of kilometers to a fraction of the size of an atomic nucleus. The frequency range is divided into separate bands, and the electromagnetic waves in each frequency band are called by different names; starting at the end of the low frequency (long wavelength) spectrum are radio waves, microwaves, infrared radiation, visible light, ultraviolet radiation, X-rays and gamma rays at the high-frequency end (short wavelength). Electromagnetic waves in each of these bands can have different properties, such as the method of their creation, the interaction with matter, and their practical use. The limit for long wavelengths is practically unlimited, and it is assumed that the limit for short wavelengths is close to the Planck length [2]. Gamma radiation, X-rays, and ultraviolet radiation are classified as ionizing radiation because their photons have enough energy to ionize atoms, causing chemical reactions. [3]

In most of the above frequency bands, it is possible to use a technique called spectroscopy to physically separate the waves of different frequencies, which creates a spectrum showing the fundamental frequencies. [3]

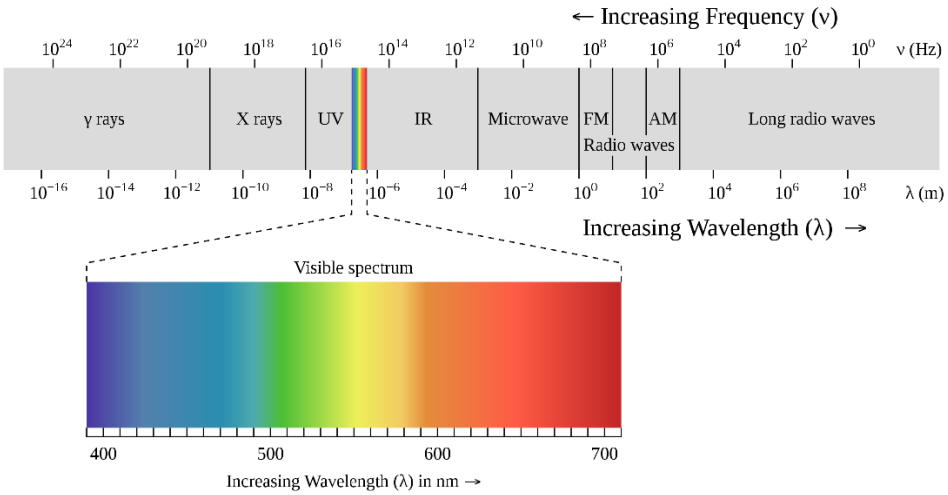

1.1. Figure: Electromagnetic spectrum [4]

When dealing with particles themselves, such as photons or electrons, the commonly used unit of energy is electronvolt (eV). One electronvolt is the energy needed to increase the electron over 1 volt, i.e., a photon with an energy of 1 eV = 1.602 × 10-19 J.

Therefore, we can rewrite the above for hc to eV:

hc = (1.99 × 10^{-25} jouls/m) × (1ev / 1.602 × 10^{-19} jouls) = 1.24 × 10^{-6} eV/m [1]

1.2. Photon flux

Photon flux can be defined as the number of photons per second per unit area. The flux of photons is essential in determining the number of electrons generated and thus the current produced from the solar cell and module. The photon flux does not provide information on the energy of the photons themselves, so the energy and the wavelength of the photons in the light source must be considered as well. With a given wavelength, it is possible to use a combination of the wavelength or energy of the photon and the flux of the photons at that wavelength to calculate the power density for photons at a particular wavelength. Power density can be calculated by multiplying the photon flux by the energy of one photon. Because the photon flux indicates the number of photons incident on the surface at a given time, multiplying the energies of the photons containing the photon flux yields the energy incident on the surface per unit time, which is equal to the power density. For determining the power density in units of W/m^2, the photon energy has to be in Joules. [1]

This photon flux of high energy (or short wavelength) photons needed to give a specific power density has to be lower than the photon flux of low energy (or long-wavelength) photons required to provide the same power density. Regarding the radiant power density incident on the surface is the same for both the blue and red light, but fewer photons from the blue band are needed since they have more energy. [1]

1.3. Spectral irradiance

Spectral irradiation is the irradiation of a surface for a given unit frequency or wavelength. It depends on whether we take the spectrum as a function of frequency or wavelength. These two forms have different dimensions, which are: the spectral irradiance of the frequency spectrum measured $W{\cdot}m^{-2}{\cdot}Hz^{-1}$, and the spectral irradiance of the wavelength spectrum measured in $W{\cdot}m^{-3}$ or, more often $W{\cdot}m^{-2}{\cdot}nm^{-1}$. [5]

Spectral irradiation at surface frequency $E_{e,v}$ is defined as

$$F(\lambda) = \Phi E \frac{1}{\Delta\lambda} \qquad (1)$$

$F(\lambda)$ is spectral irradiance in $Wm^{-2}\mu m^{-1}$;

Φ photon flux in $m^{-2}s^{-1}$;

E and λ are energy in joules and wavelength of the photons in meters. [5]

2. LIGHT GENERATED CURRENT

Generating current in a solar cell involves two critical processes. The first one of is the absorption of incident photons in order to form electron-hole pairs. Pairs of electron holes can be formed in the solar cell, given that the incident photon has energy larger than the band gap energy. On the other hand, the electrons (in the p-side) and the holes (n-side) are meta-stable. They will only exist on average for a period close to the lifetime of the minority carrier until they are rejoined. If the carrier recombines, then the electron-hole pair generated by the light is lost, and no current can be generated. This is

most common in cells where a p-n junction is used to separate the carriers. In organic cells, this can vastly differ. [1]

The other process is the collection of these carriers by the p-n junction, which prevents this recombination by the use a p-n junction to separate the electron and the hole pair. The carriers are being separated by the electric field present at the p-n junction. If the light-generated minority carrier reaches this p-n junction, it is moved across the junction by the electric field at the junction, at which point it has become a majority carrier. In the case if the emitter and base of the solar cell are connected, the light-generated current can flow through the external circuit. [5]

2.1. Collection probability

The collection probability defines the probability that a given carrier generated by light absorption in a cell will be collected by the junction. This probability mainly depends on the distance that a light-generated carrier must travel compared to the diffusion length. It also depends on the surface and mechanical properties of the device. If the generated carrier is more than a diffusion length away from the junction itself, then the collection probability of this carrier must be relatively low. Further away from the collection, probability drops. On the other hand, if the carrier is generated closer to a surface with higher recombination than the junction, then the carrier will recombine, and it won't generate any current. [1]

3. PHOTOVOLTAIC EFFECT

The carriers themselves does not give rise to power or current generation. To generate power, a voltage must be generated as well as a current. Voltage in a solar cell is generated by a process known as the photovoltaic effect. Light generated carriers near the p-n junction can cause a movement of electrons to the n-side. The other effect is for the holes which are moved to the p-side of the junction. When short circuited, we can observe no build up of charge, because these carriers can exit the device as light generated current. [1]

When light generated carriers cannot leave the solar cell there is a collection of these carriers which can cause an increase of electrons on the n side of the junction. On the p side of the material it will be a similar increase of holes. Separation of charge can create an electric field near the junction. However there is another electric field present at the junction therefore the net field is reduced. This field creates a barrier which prevents the flow of the forward bias current and the reduction of this field can increase the diffusion current. When a voltage is present across the junction a new equal state can be created. The current from the cell itself is the difference of the light generated current and the forward bias current. When the cell itself is put into an open circuit the forward bias increases and this creates a situation when light genearated current is balanced by the forward bias diffusion current. In this case the overall current is zero. We call this voltage required for this state open circuit voltage. [1]

3.1. Photoelectric effect

The photoelectric can be described as a process when an emission of electrons occur if electromagnetic radiation hits the material. The electrons which are emitted in this way are called photo-electrons. This phenomena is studied in solid state and quantum chemistry, also in condensed matter physics. From these studies it was

possible to describe properties of atoms, solids and molecules. Photoelectric effect has a wide range of use in devices specialized in light detection an precise electron emission. [1] [6]

Photoemission can occur from any material, it is most easily observed from metals and other conductors. It is because the process produces a charge imbalance which, if not neutralized by the current, leads to an increase in the potential barrier until the emission stops. Energy barrier against the photoemission is usually optimized by non-conductive oxide layers on surfaces of metal. Most experiments and devices effect use clean metal surfaces in vacuum tubes. The vacuum itself also helps to observe electrons as it prevents gases from blocking their flow between the individual electrodes. [7]

Because sunlight does not provide much ultraviolet light due to the absorption by the atmosphere, light rich in ultraviolet rays is used to be obtained by burning magnesium. At present, mercury lamps, ultraviolet lamps for rare gases, and sources of high-frequency plasma, ultraviolet lasers predominate. [8]

The classic setting for observing a photoelectric effect includes a light source, a set of filters for monochromatizing the light, a vacuum tube transparent to ultraviolet light, an emitting electrode exposed to light, and a collector whose voltage U_C can be controlled externally. [7]

To direct the photo emitted electrons to the collector a positive external voltage is used. Fixing the frequency and intensity of the incident radiation, the photoelectric current I_{pe} increases with an increasing positive voltage as more and more electrons are directed at the electrode. The photoelectric current reaches the saturation value if it is not possible to collect additional photo-electrons. This can only be present with increasing light intensity. [6]

All electrons except the energy with the highest energy are prevented from entering the collector with an increasing negative voltage. Negative voltage reaches a value that is high enough to slow down and stop the most energetic photo-electrons of kinetic energy K_{max} when no current is observed through the tube. This is called the stop voltage or the limit voltage U_o. The work performed by the deceleration potential when stopping the electron of charge e is eU_o, the following value $eU_o = K_{max}$ can be obtained. [7]

There is a specific minimum frequency of incident radiation below which photo-electrons are not emitted for a given metal surface. This frequency is called the threshold frequency. Increasing the frequency of the incident beam can increase the maximum kinetic energy of the emitted photons and the stop voltage must increase as well. The number of emitted electrons can also vary, because the probability that each photon leads to the emission of an electron is a function of the energy of the photons. Increasing the intensity of the same light, unless the intensity is too high, increases the electron ejection rate. The kinetic energy of the photo-electrons and the stop voltage will remain the same. For a given material and the frequency of incident radiation, the rate of photo-electron emission can be written as proportional to the intensity of the incident light. [6]

Time delay (less than 10^{-9} seconds) between the emission of the photo-electron and the impact of radiation is very small. Such as atomic and molecular orbital symmetry

and the electronic structure of the crystalline solids band the angular distribution of photo-electrons is highly dependent on the polarization of the incident light and the quantum properties of the emitting material. Experimental techniques that can provide data on distributions to derive material properties is called angular resolution photoemission spectroscopy. [7]

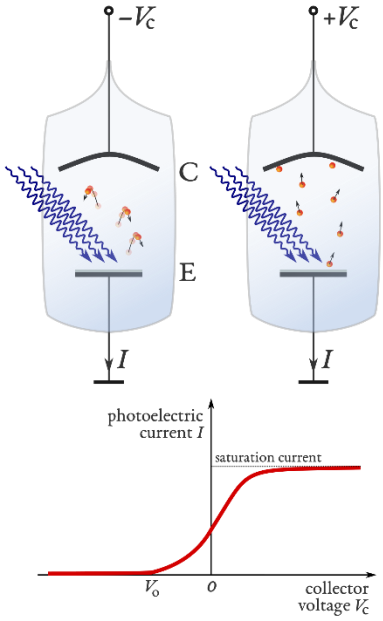

3.1. Figure: Photoelectric experiment scheme [6]

Einstein proposed the theory of the photoelectric effect in 1905 using a concept first proposed by Max Planck. Based on his studies light consists of small packages of energy known as photons or light quanta. These packets carry an energy hv, which is proportional to the frequency v for the matching electromagnetic wave. The maximum of the kinetic energy of electrons that supplied energy before they were removed from the atomic bond can be written as

$$K_{max} = hv - W \quad (2)$$

where W is the minimum energy required to remove the electron from the surface of the material. [9]

4. SPECTRAL RESPONSE

4.1. Quantum efficiency

The term quantum efficiency may refer to the ratio of incident photons to converted electrons of a photosensitive device or may refer to the TMR effect of a magnetic tunnel coupling. [1]

In a photodetector, this is the ratio between the number of charge carriers collected at any terminal and the number of photons incident on the photoreactive surface of the device. As a ratio, QE is dimensionless but is closely related to sensitivity, which is expressed in amperes per watt. The energy of a photon is inversely proportional to its wavelength, quantum efficiency is measured over a range of different wavelengths to describe the efficiency of the device at each energy level of the photon. As QE drops for solar cells to zero for photons whose energy is below the band limit. For example film typically has a quantum efficiency of less than 10%, while CCDs can have a value of more than 90%. [1]

4.2. Ideal spectral response

The definition of spectral response is the following. It is the ratio of the current generated by the solar cell to the power incident on the solar cell.

The ideal spectral response at large wavelengths is limited by the inability of the semiconductor to absorb photons with energies below the band. This limit is the same as the limit found in the quantum efficiency curves. However, unlike the square shape of the quantum efficiency curves, the spectral response decreases at small photon wavelengths. No energy above the energy of the gap in the band is used by the solar cell and instead goes to the heating of the solar cell. At small wavelengths, each photon has large energy, thus reducing the ratio of photons to power. A significant loss of energy in solar cells consisting of a single p-n junction can be present as a consequence of the inability to fully utilize the incident energy at high energies and the failure to absorb low energies of light. [1]

Spectral response and quantum efficiency are used in the analysis of solar cells depending on the application In which the examination is present. The spectral response uses the power of light at each wavelength, while the quantum efficiency uses the flux of photons. The conversion of QE to SR can be done using the following formula [1]:

$$SR = \frac{q\lambda}{hc} QE \qquad (3)$$

$$SR(\text{A/W}) = \frac{QE \cdot \lambda(\text{nm})}{1239.8} \qquad (4)$$

$$SR(\text{A/W}) = \frac{QE \cdot \lambda(\mu\text{m})}{1.2398} \qquad (5)$$

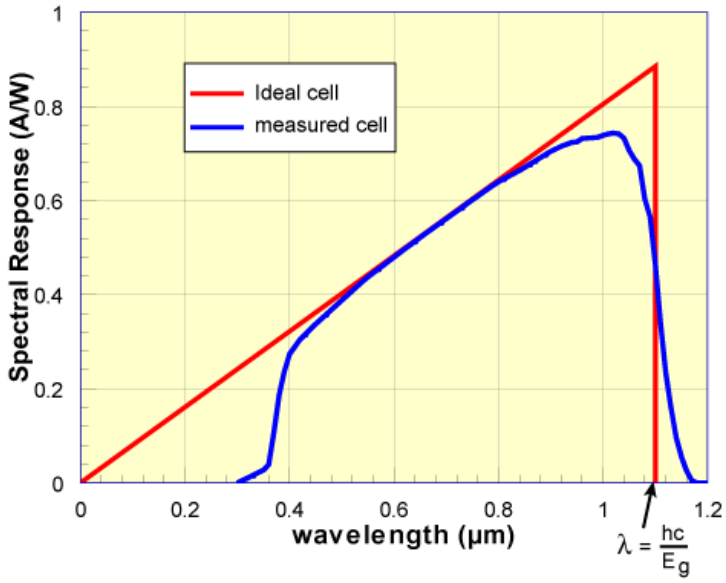

4.1. Figure: Spectral response of Si-m solar cell under glass [1]

4.3.AM 1.5 spectrum

The solar spectrum can vary during the day and with the location. Standard reference spectra are defined to allow comparison of the performance of PV plants from different manufacturers and research laboratories. Standard spectra were upgraded in early 2000 to increase resolution and international coordination of standards. The previous solar spectrum, ASTMG159, was removed in 2005. In most cases, the difference between the spectra has little effect on the device's performance, and newer reference spectra are much easier to use. [10]

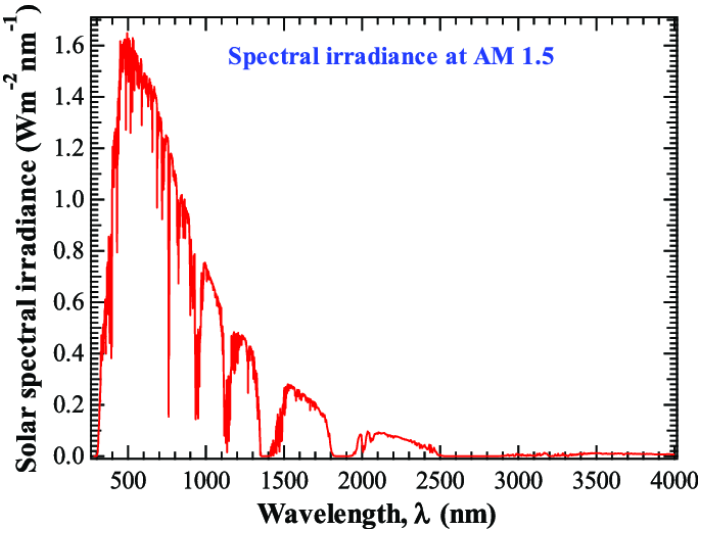

4.2. Figure: AM 1.5 spectra [11]

The more atmosphere through which it passes, the greater the attenuation. Solar radiation matches a black body radiator near 5,800K.

When the sunlight travels through the sky and the atmosphere, an interaction between the chemicals and the sunlight takes place. During this specific wavelengths are absorbed while changing the level of intensity of short-wavelength light reaching the surface. The water vapor plays a big role in this, which results at many wavelengths in a variety of absorption bands. For example molecular nitrogen, oxygen and carbon dioxide even add to this particular process. Until the reach of the surface, the spectrum is shrinked between the far-infrared and near-ultraviolet. [12]

This effect increases with a greater distance in the atmosphere through which the sunlight travels. This is why the Sun can look orange or red at dawn. More of the greens and blues are removed from the direct rays, giving an orange or red appearance to the Sun itself. For the sky which appears pink, it can be described because the green and blue bands are scattered over long paths so that they are highly changed before arriving at the observer. This can result in characteristic pink skies sunset. In removing higher frequencies from sunlight therefore scattering it atmospheric scattering can play a role as well. Because of this the sky appears blue and the Sun yellow. Blue light with higher frequency arrives at the observer with indirect scattered paths and less blue light usually follows a direct route, giving the Sun a yellow color. **[12]**

For a length L of path through the atmosphere and solar radiation incident at angle z relative to the normal to the surface, than air mass coefficient can be written as:

$$AM = \frac{L}{L_0} \qquad (5)$$

where L_0 is the path length at zenith (i.e., normal to the Earth's surface) at sea level.

The AM number is therefore highly dependent on the Sun's elevation path and as it is known it can vary with time of day, the passing seasons of the year, and also with the latitude of the observer. [12]

AM1.5, or otherwise 1.5 atmosphere thickness, is defined to a solar zenith angle of z=48.2°. Illuminance for daylight under AM1.5 is given as 109,870 lux (corresponding with the AM1.5 spectrum at 1000.4 W/m^2). The summertime air mass number for mid-latitudes during the middle parts of the day is often less than 1.5. Higher values can be observed in the morning and evening also at other times of the year. Because of this, AM1.5 is helpful to represent the overall yearly average at mid-latitudes. Concrete value of AM1.5 has been selected in the early 1970s for standardization reasons. Since then, the whole solar industry has been using AM1.5 for all standardized measurements, experiments or rating of solar cells or modules. Even with those used in concentrating systems are among this type of evaulation. The newest AM1.5 standards in photovoltaic applications are the ASTM G-173 and IEC 60904. These are all derived from simulations obtained in coherence with the SMARTS code. [13]

4.4. Measured spectral response

The method is based on the measurement of the local short circuit current I_{sc} in the cell. The external quantum efficiency can be determined from the measured short circuit current, via the formula [14]:

$$QE_E = \frac{I_{sc} \cdot h \cdot \frac{c}{\lambda}}{P \cdot q} \qquad (6)$$

where P is the laser power and λ the wavelength.

The measured spectral response can be used to predict the expected short-circuit current density. We simply calculate it on the basis of integration over the spectral range of the tested cell.

$$J_{SC} = \int S_t(\lambda) \cdot E_0 \cdot d\lambda \qquad (7)$$

where, J_{SC} is in $A * m^{-2}$, $S_t(\lambda)$ is the spectral response in $A{*}W^{-1}{*}nm^{-1}$ a $E_0(\lambda)$ is the AM 1.5 reference spectra in $W{*}m^{-2}{*}nm^{-1}$.

5. COMMON TYPES OF SOLAR CELLS

Close to 90% of the world's photovoltaics are based on some variation of silicon. The same percentage of the domestic solar module systems use crystalline silicon cells. Crystalline silicon cells can be also divided into two main categories mono and polycrystalline cells. [15]

Purity of Si molecules and the levels of efficiency are connected. Silicon can take many different forms in solar cells. The most important part is the purity of the silicon itself, which can have a direct impact on the efficiency. Purity is the way in which the silicon molecules are aligned. The better this alignment is, the purer the resulting silicon is In the end. It can provide a better capapibilty of converting sunlight to electrical power. However, efficiency is most of the time not the main focus for people who want to invest in solar energy. Usually the cost and the amount of and the dimensions of the product are the most essential aspects to potential buyers. [15]

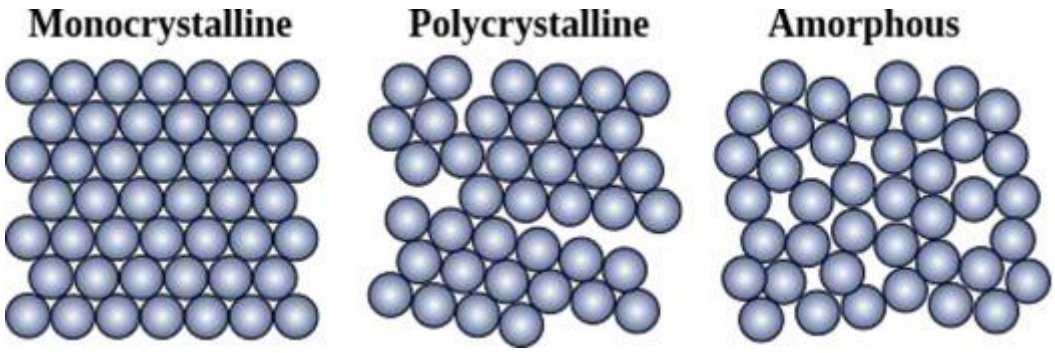

5.1. Figure: Different types of Si structures used in photovoltaics [16]

5.1.Monocrystalline cells

Monocrystalline solar cells can be made from single crystalline silicon. They are very different or recognizable in their appearance as they have a dark blue, almost black color, and the cells hold a pseudo-square shape. In order o keep the costs low and performance at optimal levels, manufacturers cut out the four sides of the cylindrical monocrystalline cells. This gives them their recognizable appearance. [15]

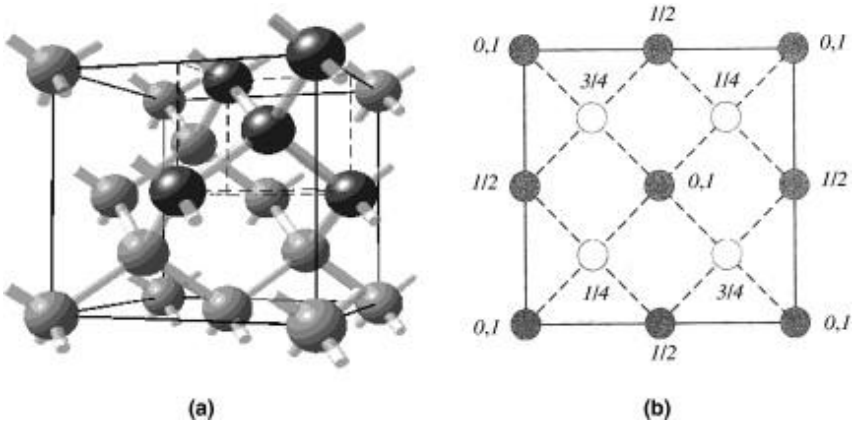

5.2. Figure: The diamond crystal lattice of silicon. (a) Spatial illustration with covalent bonding and (b) projection view. [11]

- Because of their high efficiency less space is required
- One of the longest life expectancy is given to these cells, in some cases 30-year warranty
- Perform better in low levels of sunlight - ideal for cloudy areas
- Very expensive types of cells
- With higher temperatures the performance tends to decrease
- During the manufacturing there is a lot of waste

5.2.Polycrystalline Solar Cells

The polycrystalline solar modules were introduced around the 1980s. Compared to monocrystalline cells, polycrystalline do not require each of the four sides to be cut. Polysilicon can be produced from metallurgical grade silicon by a chemical purification process, which is called the Siemens process, later this is followed by other processes involving the production of Si-m and Si-p cells. This Siemens process involves the distillation of volatile silicon compounds and their high temperatures decomposition into silicon. A process of refinement which uses a fluidized bed reactor is emerging as well. The photovoltaic industry also produces metallurgical-grade silicon. In this case the use of metallurgical instead of chemical purification processes is present. In the industry of electronics, polysilicon contains impurity levels of less than one part per billion, on the other hand polycrystalline solar grade silicon is usually less pure. [15] [17]

Polycrystalline silicon is very important in silicon-based photovoltaic industry and is used for the production of the most conventional solar cells. Close to half of the world's supply of polysilicon was being used by PV manufacturers. [17]

— The manufacturing process is cheaper and more accessible than the monocrystalline cells
— It avoids silicon waste
— High temperatures don't have as big effect on the performance of the cells. Warmer areas can utilize this.
— Efficiency is around 18 % and higher
— They have lower output rates which make them less space-efficient. So more roof space is needed for installation [15]

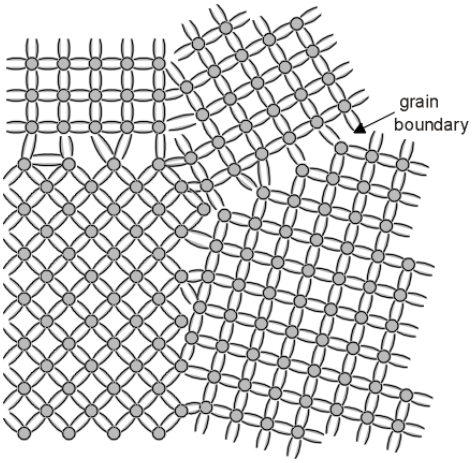

5.3. Figure: Polycrystalline silicon structure [1]

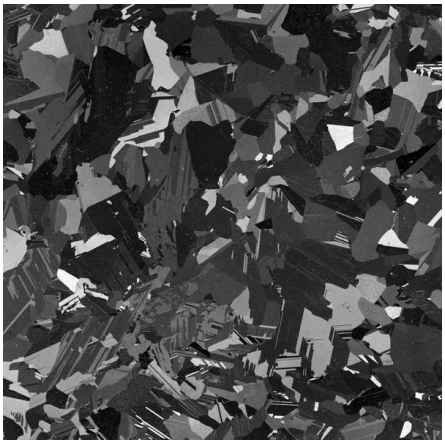

5.4. Figure: A 10 x 10 cm^2 multicrystalline wafer. The wafer has been textured so that grains of different orientation show up as light and dark [1]

5.3. Comparing Monocrystalline and polycrystalline cells

In monocrystalline silicon, the crystalline lattice is homogenous, recognized by an even external coloring. The sample is usually one single and continuous crystal as its structure which contains no grain boundaries. It can also be challenging to produce large single crystals (which are rare in nature) in the laboratory. On the other hand, in an amorphous structure, the order in atomic positions is limited to short range. [17]

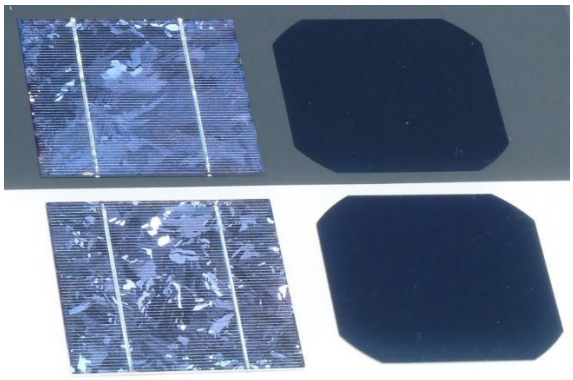

5.5. Figure: Comparing polycrystalline (left) to monocrystalline (right) [17]

5.4.Thin-Film Solar Cells

There are several types of thin-film solar cells, and how they differ from each other is essentially connected to the material used for the PV layers. Thin-film solar cells are manufactured by placing several thin layers of photovoltaic material on top of each other to creates the module. Types can be the following:

- Amorphous silicon [18]
- Cadmium telluride
- Copper indium gallium (di)selenide (CIGS)
- Organic PV cells

The efficiency rates for these solar cells depending on the technology used tend to move between 18 % to 21%. The polarity for thin-film solar cells have risen dramatically since 2003, which means that research and development have increased. On the other hand, an increase in demand for crystalline cells has lowered the price for these cells and the need and development for thin-film cells. [15]

- It is possible to manufacture them to be flexible, whis way they can be applicable to a range of situations and building types
- Mass production is available easily
- On efficiency shading has abig effect
- They can take up a lot of space
- Low space-efficiency means that they will cause further expenses in the form of enhancers, like cables or support structures
- They have a shorter lifespan and less good warranty conditions

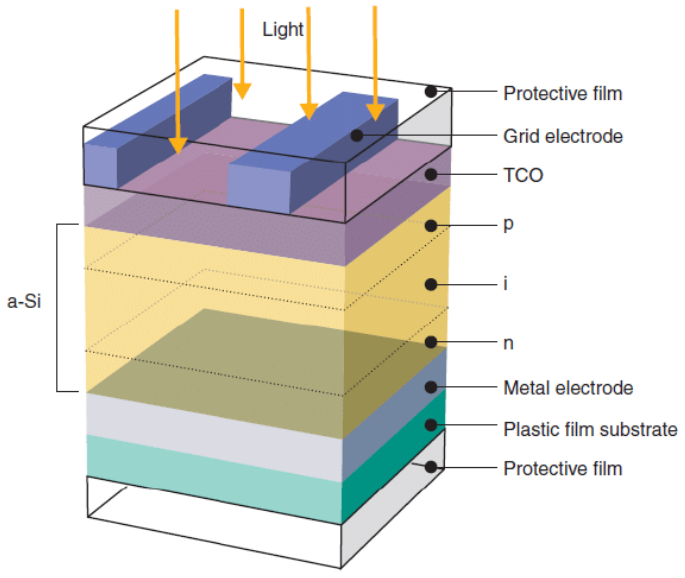

5.6. Figure: Amorphous silicon solar cell device structure [11]

6. MISMATCH EFFECTS

Mismatch effects are usually caused by the interconnection of solar cells or modules. These connections do not have the same properties or they have different conditions. Big problem for PV panels are non-compliance losses under certain states because the performance of the entire module under the least favorable conditions is determined by the solar cell with the lowest output. When one solar cell is shaded while the rest is not in the module, the energy generated by not covered solar cells can be dissipated by a lower power cell rather than a load supply. This, in turn, can lead to highly centralized and localized energy dissipation, and the resulting local heating can cause irreversible damage to the module. [1]

A mismatch in the PV modules occurs when the electrical parameters of one solar cell change significantly from the parameters of the remaining devices. The impact and loss of power due to non-compliance depend on:

- circuit configuration
- the operating point of the PV module [1]

Differences in any part of the V-A curve between one solar cell and another can lead to losses at a particular operating point. The following figure is a non-ideal curve IV and operating mode of the solar cell. Although a mismatch may occur in any of the cell parameters, significant mismatches are most often caused by differences in either the short-circuit current or the open-circuit voltage. [1]

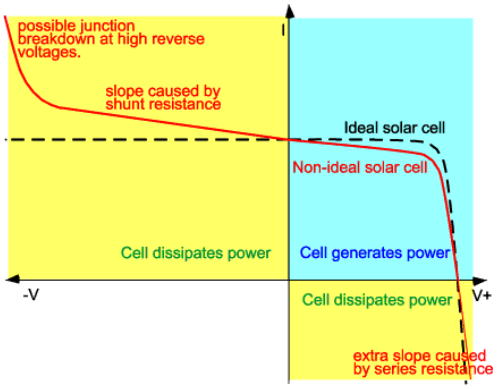

6.1. Figure: Comparison of ideal and non-ideal solar cell [1]

The mismatch factors can also show up at the cells within a given module with different spectral responses.

7. METHODS OF MEASURING RELATIVE SPECTRAL RESPONSIVITY

The relative spectral responsivity of a photovoltaic component is measured by irradiating the photovoltaic component with a narrowband light source in a series of different wavelengths covering its sensitivity range and measuring the short-circuit current and irradiance at each of these wavelengths.

7.1. Monochromator

One way to measure spectral sensitivity is to use the monochromator shown in the figure. At inlet A there is a radiation source, which is directed by means of a slit B to a curved mirror C, which directly reflects the radiation on the prism D.

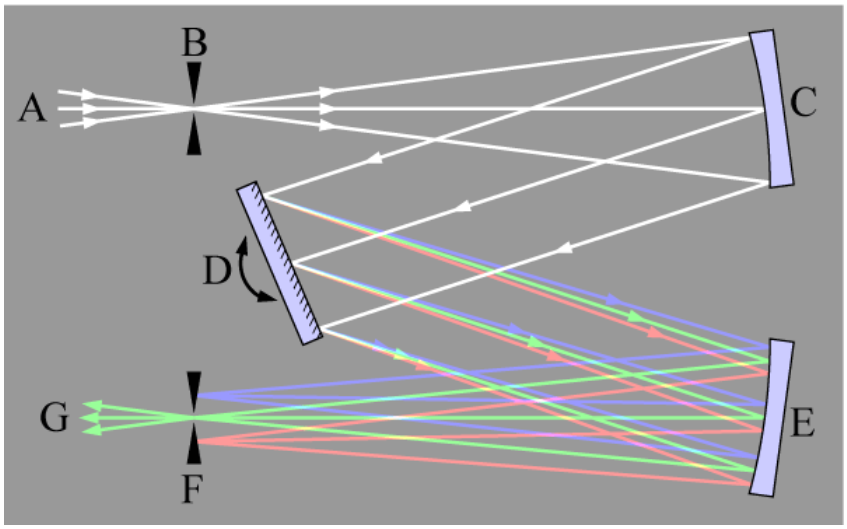

7.1. Figure: Concept of a monochromator [19]

Then, the reflected light, where each wavelength has a different angle of reflection, is reflected to the mirror E, which directs all the rays into the slit F. Depending on the rotation of the mirror E, only a ray of the desired wavelength penetrates the slit F.

7.2. Spectral filters

Another type of measurement can be done by using a light source and individual color filters, which can be used to set the desired wavelength. In optics, there are several basic types of filters according to spectral properties. These are edge filters, bandpass filters, bandpass filters, conversion filters, special and non-selective filters. Edge filters are characterized by high transmittance for the long-wavelength range, and from a particular wavelength there is a sharp transition and absorption of shorter wavelengths. Transmission bandpass filters, as the name suggests, transmit light in a narrow wavelength band, and light is absorbed on both sides of the band.

Retention bandpass filters are the exact opposite of leakage bandpass filters. Their aim is to filter a certain wavelength band and pass the rest of the spectrum, and they are used e.g. To eliminate UV radiation. Conversion filters are characterized by a gradual increase (redness), or decrease in wavelength. Special filters are used with uneven spectra, frequent local extremes, which aim to filter out selectively. From the spectrum, it is possible e.g. filter out the source of artificial radiation. The last type is

the so-called non-selective filters, which are also called neutral. Their goal is to absorb excess light without affecting the distribution of the spectrum.

From the use of filters described above, it is clear that this method is financially and time-consuming because it is necessary to purchase more than one filter to determine any wavelength. With the increasing variability of more wavelengths, not only the price increases but also the time consuming, which manifests itself primarily in the more frequent alternation of the required wavelength, when it is necessary to replace the individual filters.

7.3. Continuum lasers

Continuum laser is a laser whose operating wavelength can be changed in a controlled way. While all laser gain media allow small shifts in the output wavelength, only a few types of lasers allow continuous tuning over a wide range of wavelengths and give the user great flexibility with measurements.

The first truly widely tunable laser was a color laser in 1966. Hänsch introduced the first tunable narrow line laser in 1972. Color lasers and some semiconductor lasers have huge bandwidths, allowing tuning in the tens to hundreds of nanometers range. Titanium doped sapphire is the most common tunable semiconductor laser capable of laser operation from 670 nm to 1100 nm. These laser systems typically include a Lyot filter into the laser cavity that rotates to tune the laser. Other tuning techniques include diffraction gratings, prisms, standards, and combinations thereof. The multi-prism grating arrangement in several configurations is used in diode, dye, gas, and other tunable lasers. [20]

7.3.1. Single line tuning

Because no laser is truly monochromatic, all lasers can emit light in a range of frequencies, referred to as the laser transition line width. In most lasers, this line width is relatively narrow (for example, the 1064 nm wavelength transition of an Nd: YAG laser has a line width of approximately 120 GHz or 0,45 nm). Tuning the laser output in this range can be achieved by placing wavelength-selective optical elements (e.g., a standard) in the laser's optical cavity to ensure the selection of a particular longitudinal mode of the cavity. [20]

7.3.2. Multi-line tuning

Most laser gain media have a number of short wavelengths at which laser operation can be achieved. For example, Nd: YAG, like the main output beam at 1,064 nm, has weaker transitions at 1052 nm, 1074 nm, 1112 nm, 1319 nm, and a number of other bands. Usually, these beams do not work unless the gain of the most robust transition is suppressed, e.g. using wavelength-selective mirrors. If a dispersing element, such as a prism, is introduced into the optical cavity, the inclination of the cavity mirrors can cause the laser to tune, which moves between different laser lines. Such schemes are typical in argon-ion lasers, which allow the laser to be tuned to a number of lines from ultraviolet and through blue to green wavelengths. [20]

7.3.3. Narrowband tuning

With some types of lasers, it is possible to adjust the length of the laser cavity, thereby continuously tuning them over a wide range of wavelengths. Semiconductor Distributed Feedback Lasers (DFBs) and Vertical Cavity Surface Emitting Lasers (VCSELs) use periodically distributed Bragg reflector structures (DBRs) to create optical cavity mirrors. If the temperature of the laser changes, a change in the index of the DBR structure will cause a shift in its peak reflection wavelength, and thus in the laser wavelength. The tuning range of such lasers is usually a few nanometers, up to a maximum of about 6 nm, as the laser temperature varies around ~ 50 K. In principle, the wavelength for DFB lasers is tuned by 0.08 nm/K in wavelength mode 1550 nm. Such lasers are commonly used in optical communication applications, such as DWDM systems, which allow the wavelength of a signal to be adjusted. [20]

7.4. Continuum laser - SuperK Extreme

SuperK Extreme from NKT Photonics is an effective supercontinuum laser in the industry. High efficiency comes with better reliability and less unwanted residual output power.

7.2. Figure: SuperK Extreme supercontinuum laser [21]

- With a wavelength range from 400 to 2400 nm, SuperK lasers are low-noise, wideband sources designed for optical coherence tomography. Optical coherence tomography in the visible wavelength range as well as in the region of 1300 nm. Thanks to their vast output and low noise, SuperK supercontinuum lasers are the ideal source of OCT when you need resolution in microns or when you need a unique range of wavelengths. [21]
- Paired with a broadband spectrometer, these sources provide the same performance as Ti: Sapphire-based OCT systems at a much lower cost, less footprint and outstanding robustness. [21]

7.5. SUPERK VARIA tunable filter

SuperK VARIA is an efficient and flexible alternative to the monochromator, which effectively converts the SuperK supercontinuum laser into a powerful single-line laser with a tuning range of 440 nm and with variable bandwidth. The center wavelength of the passband can be tuned anywhere between 400 and 840 nm, and the bandwidth is variable between 10 and 100 nm. Increasing the filter bandwidth has other advantages in the form of higher energy throughput and fewer spots in imaging applications. In addition, high out-of-band suppression of up to 50 dB makes the SuperK VARIA an ideal tool for FLIM and other applications using high-sensitivity detectors. SuperK VARIA is designed for use with super-continuous SuperK sources but can also be used with traditional laser systems or broadband light sources. [22]

7.3. Figure: SuperK VARIA tunable filter from NKT Photonics [22]

7.6. Light Beam Induced Current (LBIC)

LBIC technology is based on electrical current measurement. A laser beam is shined on the sample in one point and creates an electrical current which is measured by the tool and represents the short circuit current (ISC) at the given illumination. The reflection (R) of the multiple laser source is sensed by the reflection detector. The ISC and reflection values can be determined by the internal quantum efficiency (IQE). Using multiple wavelengths, the diffusion length can be measured. [23]

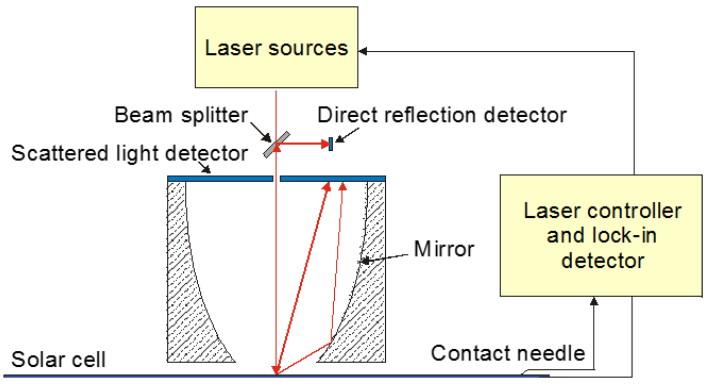

7.4. Figure: Light beam induced current (LBIC) method setup [23]

8. EXPERIMENTAL PART

One of the main goals of this thesis was to measure the spectral responsivity of different types of solar modules with the use of specific wavelength lasers which were available and later determine the characteristics of each type. Furthermore to evaluate the homogeneity of the spectral response of these different types of solar cells. Measurements using the continuum laser couldn't been done due to the coronavirus pandemic and the restrictions due to it. This put the experimental part up for a challenge but in the end this was done partly at the Polytechnic University of Valencia (UPV) and at the Polytechnic City of Innovation (CPI) in Spain.

Measuring the spectral responsivity of a given solar cell as discussed in the theoretical part by this method involves measuring the light induced short circuit current in the cell, which is produced through appropriate excitation. For the measurement, the solar cell is prepared and irradiated at specific points with laser light of specific wavelengths.

8.1. Measuring apparatus and methods

A variety of spectral response measurement systems have been designed by the PV community, including methods based on interference filters, grating monochromators, and interferometers. Determining the measuring apparatus and its parts in this thesis involved a few key aspects. Firstly, it was essential to execute the measurements as precisely as possible with the available equipment. Secondly, the data had to be as usable as in standard methods for measuring spectral responsivity like the Light Beam Induced Current (LBIC) approach.

The quantum efficiency is typically measured with bias light simulating reference conditions because the device may be nonlinear. Typically, the spectral correction factor for efficiency measurements is calculated based on QE measurements near 0 V and is assumed to be the same as at the maximum power point. This assumption is valid for most PV systems and results in a negligible error for amorphous silicon, which has a voltage-dependent spectral responsivity.

In our case, three lasers were used with different wavelengths, similar to the technique used by LBIC. These commonly used RGB lasers had a wavelength of 635,2 nm, 532 nm, and 447,9 nm respectively, with a power of $1{,}5*10^{-5}$ W. All three lasers were the same type and from the same manufacturer. The selection of these RGB lasers was mainly based on the method which was followed in this thesis. This meant that as wide a range of wavelengths as possible was needed to cover three main parts of the spectra.

In addition to these lasers, the setup consisted of mechanically attachable holders and standoffs which are often used in the field of photovoltaics. This setup ensured that the measuring table and the instruments were fixed in a particular position. It also allowed great flexibility with quick adjustments which were often needed during the measurements.

The measuring distance L between the solar cells and the laser was selected based on previous experiments of this type. In each of the experiments this distance was the same length $L = 40\ cm$.

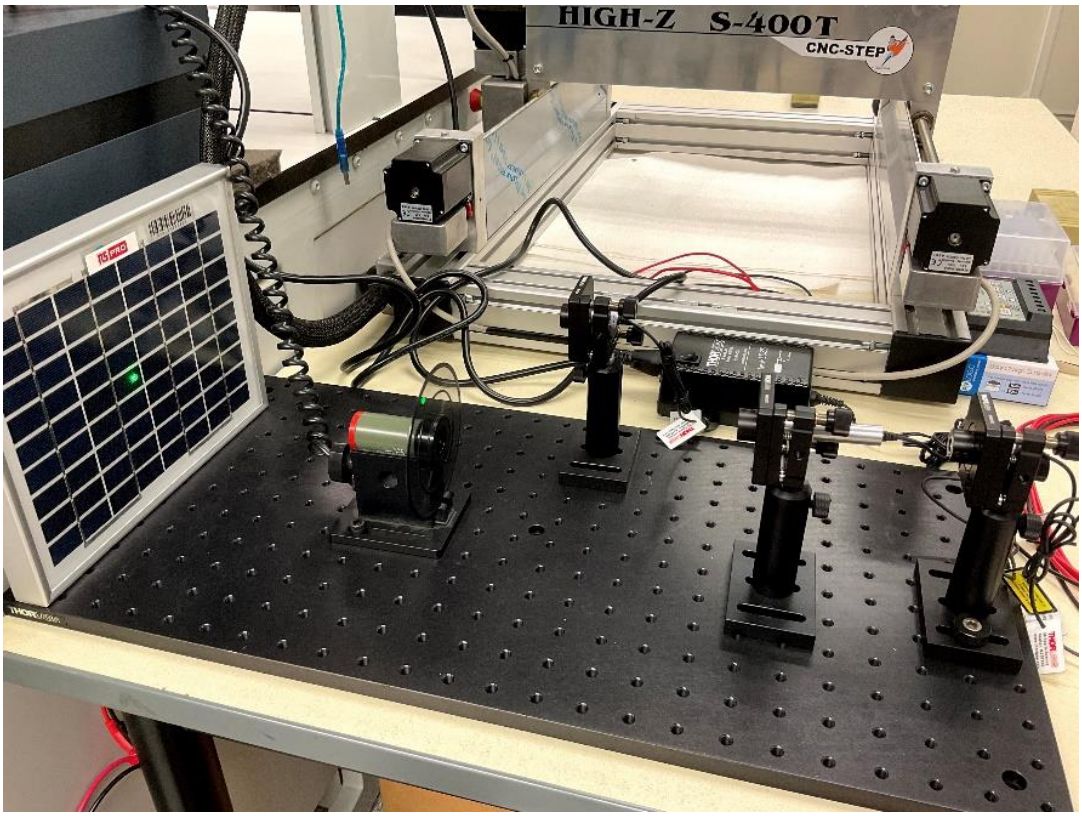

8.1. Figure: Measuring setup for the experimental part with lasers and a Si-m type solar module visible

Other important of the measuring setup was the use of an optical chopper which allowed us to filter out the background ambient light from the laser source light on our solar modules and cells. The chopper frequency was setup so that it wasn't in sync with the ambient light frequency. This way any disturbances from the ambient background light could be avoided. The optical chopper had the following parameters:

- Model and manufacturer:
  - SR540 OPTICAL CHOPPER from Stanford Research Systems, Inc.
- Frequency range:
  - 4 Hz to 40 Hz
  - 40 Hz to 400 Hz
  - 400 Hz to 3.7 kHz

In our experiments the chopper frequency was set to $f = 280\ Hz$. This value was used as a reference frequency for the lock-in amplifier to filter out the background ambient light which wasn't going trough with this exact frequency.

8.2. Lock-in amplifier method

Typically, the spectral response is measured at short-circuit current. The measured photo-current is often in the μA to mA range with a broadband DC bias light near the devices intended operating point. PV devices normally operate near their maximum power point.

It is often desirable to measure the QE of modules consisting of multiple cells in series. The simplest approach would be to illuminate the whole module with ac monochromatic and dc broadband light with the module at 0 V, just as in the case of cells.

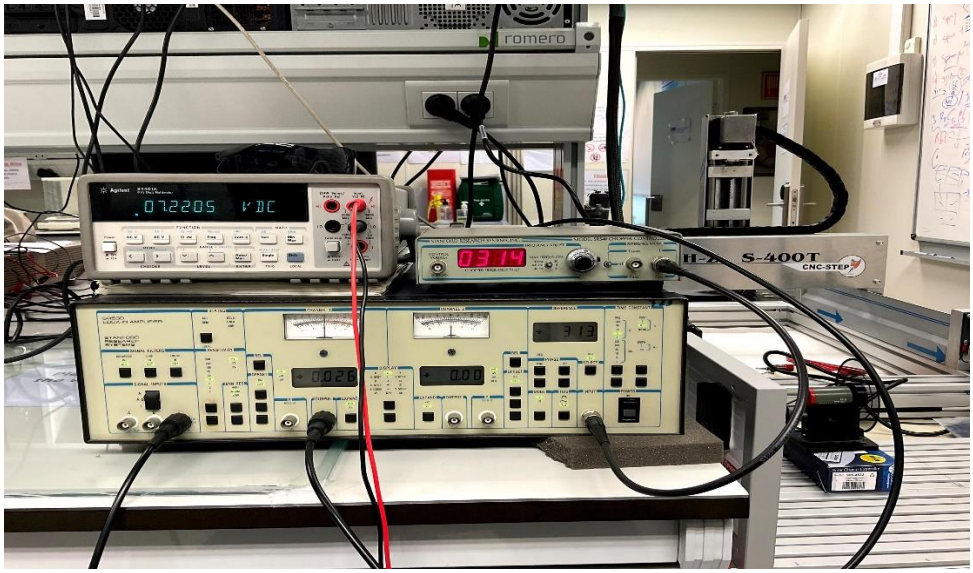

8.2. Figure: Measuring apparatus with the lock-in amplifier method

Modern digital lock-in amplifiers have rapid auto-ranging capabilities and will outperform an ac voltmeter for noisy signals.

In our experiment the SR530 Lock-in Amplifier was used from Stanford Research Systems. It has a 0,5 Hz to 100 KHz frequency range, current and voltage inputs, tracking band-pass and line filters and four ADC inputs, two DAC outputs.

8.3. Nano-amperemeter method

In this method the use of lock-in amplifier was substituted with a nano-amperemeter. All other parts of the experiment remained the same for the exception of the connection to the individual modules since it was essential to filter out the background light generated current. This was done by using two channels to the nano-amperemeter. Firstly, the bias background light was measured for the whole module, later the laser beam was applied and the values were collected again.

8.4. Measured solar cells and its parameters

Four main types of solar modules were selected for the experimental part of this thesis. The selection was partly based on the popularity of the solar modules in the industry as a whole, on the other hand it was based on modern and developing technologies in mind for ex. perovskite solar cells, which are not yet ready for production in a big scale for the reasons discussed in the theoretical part.

The first category of solar cells were silicon based mono- and polycrystalline materials. These modules were very similar to each other regarding their parameters and sizes. These were the following:

Serial Number	9046128
Nominal Peak Power (Wp)	5 W
Nominal Voltage (Vmp)	17,5 V
Nominal Current (Imp)	0,29 A
Open Circuit Voltage (Voc)	22,0 V
Short Circuit Current (Isc)	0,32 A
Operating Temperature	-40 °C to +85 °C
Maximum System Voltage	600 V DC

8.3. Figure: Paramters of Si-m and Si-polycrystalline PV modules

8.4. Figure: RS Pro Si-m solar module [24]

From the next category of solar cells amorphous silicon modules were introduced into our experiment. The size and the parameters of these modules were the following:

Part Number	8957252
Maximum power (W_p)	2,5 W
Voltage at MPP	12 V
Current at MPP	0,15 A
Open Circuit Voltage (Voc)	18 V
Short Circuit Current (Isc)	0,25 A

8.5. Figure: Parameters of the used amourphous silicon solar modules

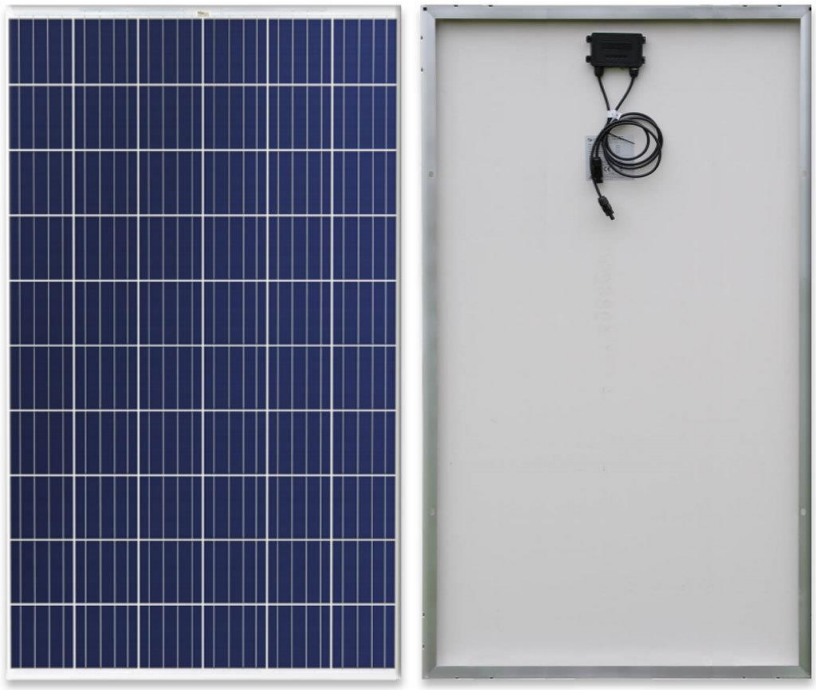

8.6. Figure: Exiom EX-150P-36 150W 12V polycrystalline solar panel [25]

The last category which was selected for our experiments were perovskite solar cells of $CH_3NH_3PbX_3$. These cells were attached to an enclosure which allowed us to measure the short-circuit current from an individual cell. This enclosure was designed and later successfully printed out on a 3D printer. As discussed previously solar cells of this type are not in a production phase yet and there is still a need for their development especially regarding the life expectancy. For this reason, the data from this cell cannot be looked at in the same way as in the other three previous types of cells.

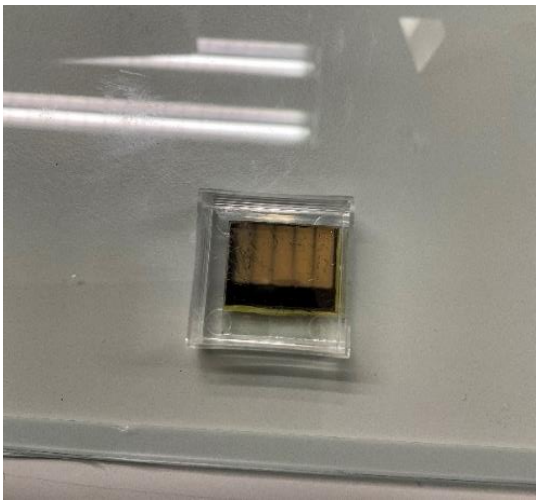

8.7. Figure: Perovskite solar cell prepared for the experiment with golden contacts

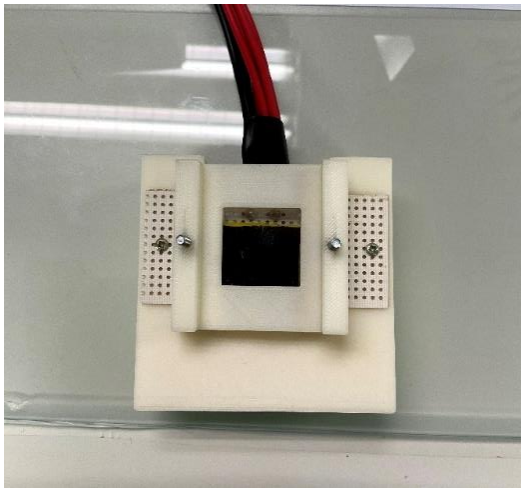

8.8. Figure: 3D printed enclosure for the perovskite solar cell with contacts

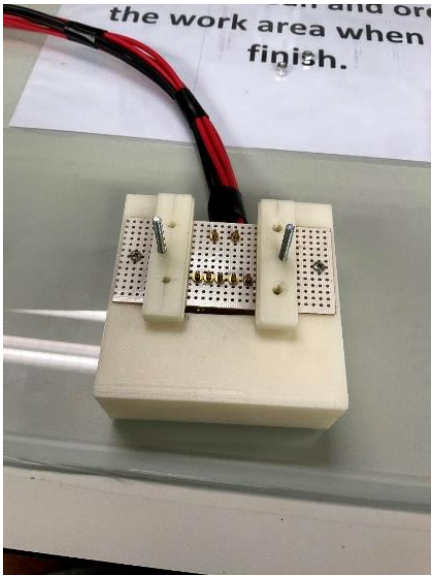

8.9. Figure: Electrical contacts visible on the 3D printed enclosure for testing perovskite solar cells

8.5. Possible sources of error

With each measurement there are errors and mistakes which can occur, and we cannot avoid them completely. In this experiment these errors could've been caused by the electrical instruments, from the PV cells and modules themselves or mechanical disturbing factors which can be present in every laboratory. These sources of errors are listed bellow divided into these three categories:

Electrical Instrumentation

- current-to-voltage (I to V) converter
- gain, linearity, noise, offset
- signal from I to V converter
- lock-in amplifier (typically < 1 mA)
- calibration, resolution, accuracy,
- waveform to sine wave correction factor,
- overloading, noise, dynamic range,
- time-constant,
- procedures for using lock-in amplifier
- a DC voltmeter
- gain, offset from noise level,
- linearity, time-constant

PV cell or module

- temperature,
- response-time to periodic light,
- linearity of PV device
- white-light bias spatial uniformity,
- monochromatic light spatial uniformity,
- voltage bias of cell being measured,
- spectral content of bias light,
- device sensitivity to polarization of light

Mechanical

- mechanical movement of optics,
- mechanical vibration,
- chopped stray monochromatic light

A big focus was placed in our experiments to avoid these errors and minimize them as much as possible. To avoid the possible mechanical errors in the distance between the laser light source and the solar cells was frequently measured and checked to ensure that no change in the distance was present. Furthermore, the light source was in a predetermined fix position which was the same for every measurement only the laser source themselves were changed.

Regarding the errors of the electrical instruments there was just a minimal flexibility in what there could have been done to avoid these as these products were mostly not suitable for modifications and some of the instruments were still under warranty from the manufacturer.

9. MEASURED DATA

In this part the measured and calculated data from the experiment will be presented and discussed. This section is divided into four parts based on the four types of solar cells and modules which were measured by our method. For each type of solar cell and module five measurements were provided with the same fixed position, which was possible with the help of an optical measuring table with screws and holders. As it was discussed previously in part 8.1. three lasers of different wavelengths were used in our experiments.

The average short circuit current Isc was calculated based on these measurements. These values of current were converted to the response R in A/W based on the power produced by each of the laser lights. Later with the help of equations which are present in the part 4.4. external quantum efficiency and spectral responsivity were calculated. Data were compared with reference spectral responsivities which were obtained from multiple sources of previous experiments of this character and type.

9.1. Lock-in amplifier method

In this part the data from the lock-in amplifier method measurements are shown. The data was imported and interpreted into tables and graphs with corresponding characteristics. The reference data shown in the graphs were obtained from literature which discusses and examines the same problematic.

9.1.1. Monocrystalline solar cells

Monocrystalline solar cells are usually sensitive in the wider aspect of the spectrum from 350 to 1150 nm. These cells can also work and produce current in the infrared part of the spectrum. These cells have much wider spectral sensitivity than what was measured with these three lasers in our experiments, nevertheless the data shows that it corresponds to the theoretical expectations in the margin of error which was a maximum of ±0,04 mA.

Measurement no.	I [mA] - R (635,2 nm)	I [mA] - G (532 nm)	I [mA] - B (447,9 nm)
1	0,67	0,62	0,56
2	0,70	0,65	0,58
3	0,72	0,66	0,59
4	0,68	0,67	0,61
5	0,71	0,65	0,59
Average Isc [mA]	0,70	0,65	0,59
R [A/W]	0,464	0,433	0,390
EQE [-]	0,905	0,845	0,761
SR [A/W]	0,464	0,363	0,275

9.1. Figure: Table with measured and calculated data for monocrystalline silicon solar cells

In the values for the external quantum efficiency, we see a trend of increasing values for higher wavelengths which corresponds to previous experiments in this field. External quantum efficiency largely depends on the optical losses for example transmission and reflection. We can correct the values of external quantum efficiency by measuring the reflection and transmission of a module, but in this case this wasn't the main goal of our experiment.

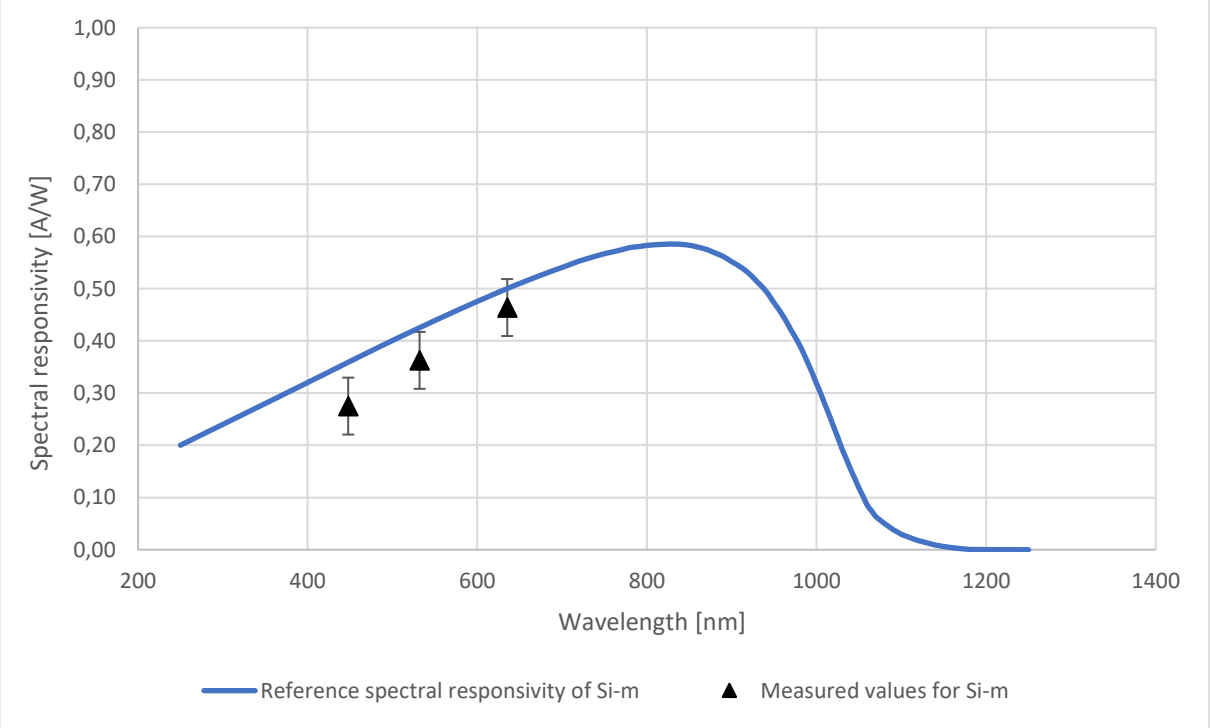

9.2. Figure: Comparing measured spectral responsivity with the reference data for monocrystalline Si cells

It is visible from figure 9.2. that the measured data for monocrystalline silicon cells corresponds with the reference curve [1] of the spectral responsivity. The value at 447,9 nm is the only exception which is lays outside from the reference curve even with its standard deviation. At the longer wavelengths we can see the response falling back to zero values. These types of cells have an indirect band gap therefore no sharp cutoff is visible at these band gap wavelengths.

The ideal spectral response has a limit at longer wavelengths because it's not capable of absorbing photons with energies under the band gap. We can see this limit appear also in EQE curves.

With energies larger than the band gap the cell cannot use the available energy, and this appears in higher cell temperatures.

This data of spectral responsivity can be used to analyze the solar cell application and decide which one of them is the most suitable for the case.

9.1.2. Polycrystalline silicon

Measurement no.	I [mA] - R (635,2 nm)	I [mA] - G (532 nm)	I [mA] - B (447,9 nm)
1	0,68	0,60	0,56
2	0,69	0,61	0,55
3	0,70	0,63	0,54
4	0,67	0,60	0,53
5	0,71	0,62	0,55
Average Isc [mA]	0,68	0,61	0,55
R [A/W]	0,456	0,408	0,364
EQE [-]	0,889	0,796	0,710
SR [A/W]	0,457	0,342	0,257

9.3. Figure: Table with measured and calculated data for polycrystalline silicon solar cells

Spectral responsivity characteristics for polycrystalline silicon cells are very similar to those what we got at the monocrystalline samples. One of the reason for this can be the fact that these two types of cells are made from the same material and such behavior is expected based on previous experiments comparing these materials. The data shows little deviation of the measured short-circuit current a maximum of ±0,03 mA. Polycrystalline cells are being more sensitive to the red band with longer wavelengths and less sensitive to the green band. These differences between the polycrystalline and monocrystalline cells can be interpreted as small. One of the possible methods of increasing the efficiency of the cells would be done by reducing cell temperature, but on the other hand we can't reduce the infrared radiation as it would mean a reduction in the efficiency of the cell. Infrared radiation and heat energy is an important part of the sunlight spectrum.

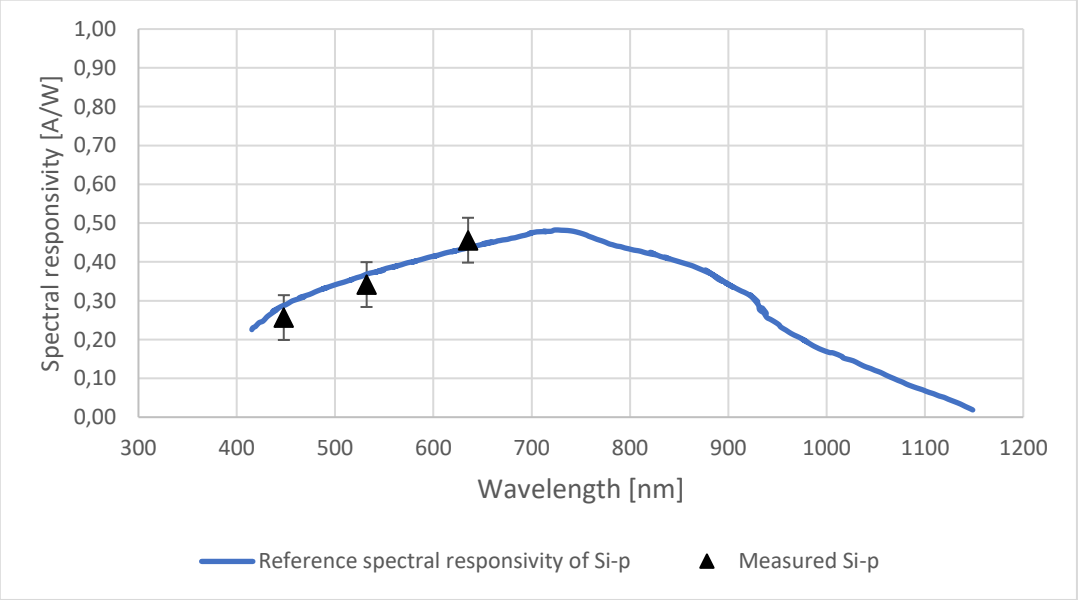

9.4. Figure: Comparing measured spectral responsivity with the reference data for Si-p cells

9.1.3. Amorphous silicon

Measuring these types of cells was more complicated due to the electrical connections which were needed to be changed out. Our goal was use the same as on the previous two mono- and polycrystalline Si cells due to the concern that to the small values of short-circuit current errors would be introduced by the different type of the connection.

Measurement no.	I [mA] - R (635,2 nm)	I [mA] - G (532 nm)	I [mA] - B (447,9 nm)
1	0,31	0,45	0,20
2	0,32	0,46	0,19
3	0,29	0,44	0,21
4	0,29	0,45	0,25
5	0,28	0,47	0,22
Average Isc [mA]	0,30	0,45	0,21
R [A/W]	0,199	0,303	0,143
EQE [-]	0,388	0,590	0,278
SR [A/W]	0,195	0,253	0,101

9.5. Figure: Table with measured and calculated data for a-Si solar cells

Amorphous silicon solar cells don't have as good spectral sensitivity as other types of solar module. Their sensitivity ends near at a wavelength of 800 nanometers. Its spectral characteristics starts at around 350 nanometers.

From the data of the measurements, we can see that all of them lay outside of the reference values [26] of the spectral responsivity. This may have been caused by the previously mentioned change of electrical connections which can cause disturbances in the lock-in amplifier setup as its very sensitive to any change in the input data from the solar cells.

One of the main advantages of amorphous silicon cells is that it allows other subtrates to be used such as steel or plastic films instead of traditional glass layers. This allows that new types of cells can be created in different shapes and forms which might have the possibility to even bend. These cells can be also used as visible light sensors as their responsivity corresponds essentially to the same wavelengths as other types of cells.

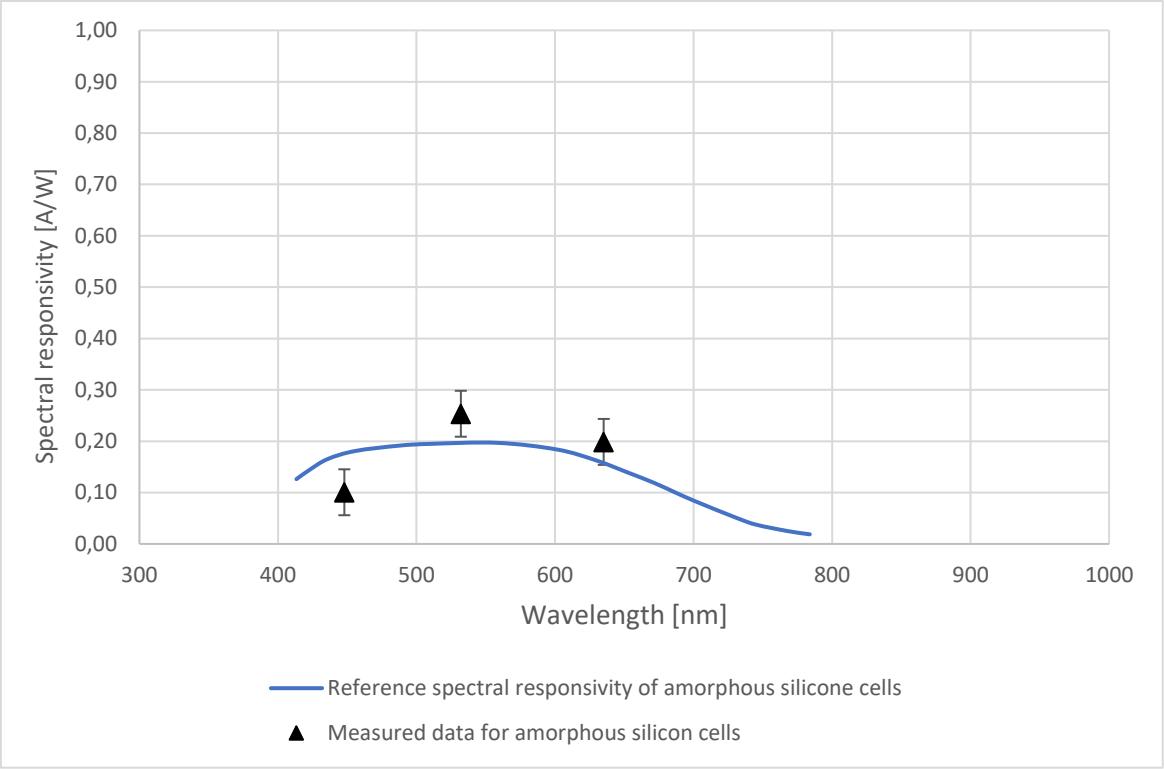

9.6. Figure: Comparing measured spectral responsivity with the reference data for a- Si cells

9.1.4. Perovskite solar cells

In the following table the measured values for each wavelength is shown for perovskite solar cells of $CH_3NH_3PbX_3$.

Measurement no.	I [mA] - R (635,2 nm)	I [mA] - G (532 nm)	I [mA] - B (447,9 nm)
1	0,60	0,55	0,42
2	0,61	0,54	0,41
3	0,59	0,50	0,40
4	0,59	0,52	0,43
5	0,59	0,53	0,41
Average Isc [mA]	**0,60**	**0,53**	**0,41**
R [A/W]	0,397	0,352	0,276
EQE [-]	0,775	0,687	0,538
SR [A/W]	**0,397**	**0,295**	**0,195**

9.7. Figure: Table with measured and calculated data for perovskite solar cells

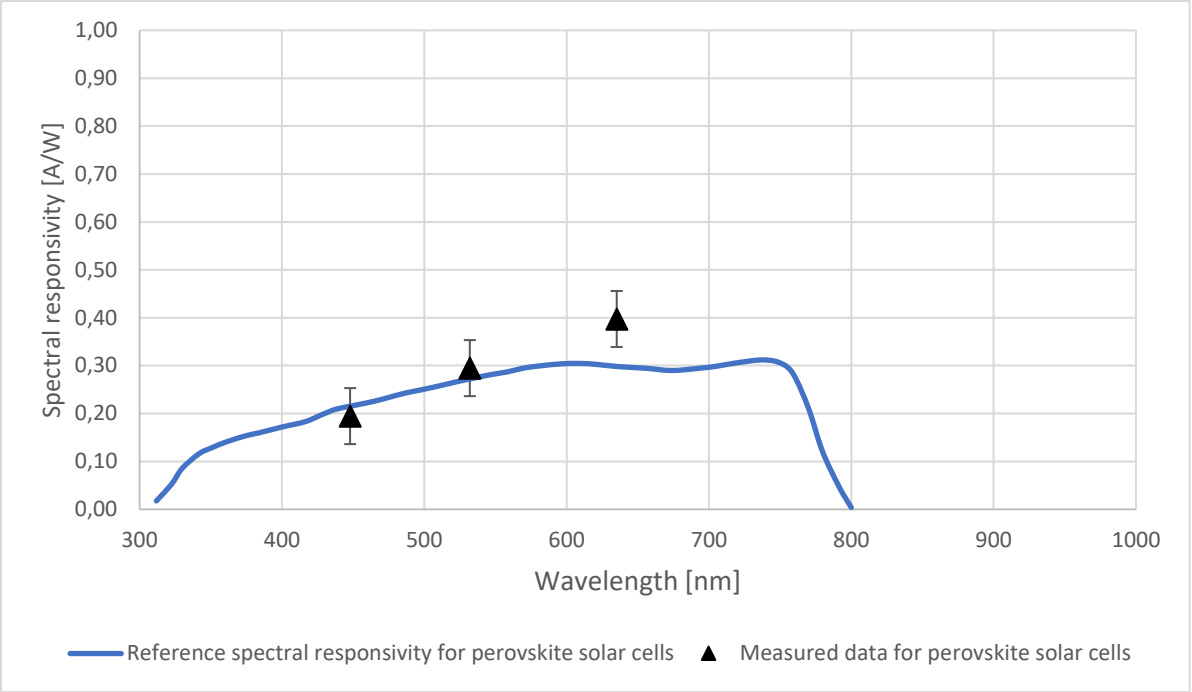

9.8. Figure: Comparing measured spectral responsivity with the reference data for perovskite cells

In the measured data for the perovskite cells we can see that it follows the reference values [27] except at the last wavelength at 635,2 nanometers. A lower sensitivity is visible at lower wavelengths near the blue band. This reduction continues until around 300 nanometers were no significant responsivity can be measured from the cell based on the reference data [27]. At higher wavelength near the red band we can observe that a stable region is present for the spectral responsivity. This ends near 760 nanometers after which a big reduction in responsivity is present ending at 800 nanometers with 0 responsivity.

During the measurements it was shown that the frequency of the chopped light had a significant impact on SR measurements with perovskite cells. The wavelength characteristics of perovskite device types as detailed in figure 9.8 shows that the optimal setting for the chopper frequency was 280 Hz. It was also shown from our experiments that change in the frequency caused just a shift in the absolute scale of SR the shaped changed just by a small extent.

The short-circuit measurements depend heavily on the background irradiance conditions. This influence was visible not just at the examined perovskite cells but at all of the other types of cells. From the measurements it was visible that a consistent bias background light should be used for ex. by a solar simulator and a load of 0V to obtain more precise data of Isc.

Overall, this method could be used to increase accuracy of the data and improve the SR scale of measurement for even higher wavelengths.

9.2. Nano-ampere method

In this section measured data with the nano-ampere method are shown divided into subsections of each examined materiel and type of solar module. The data as in the previous case were imported into tables and the values for external quantum efficiency and spectral responsivity were calculated. For each type of material and table set of graphs were constructed with reference data from different sources of experiments in this regard.

We expected more precise results from this method due to the smaller error gap of the measuring device. As it was visible from our measurements in the end this method didn't provided us the level of confidence as in the lock-in amplifier method.

9.2.1. Monocrystalline silicon

Measurement no.	I [mA] - R (635,2 nm)	I [mA] - G (532 nm)	I [mA] - B (447,9 nm)
1	0,69	0,61	0,56
2	0,71	0,58	0,57
3	0,70	0,55	0,58
4	0,67	0,54	0,56
5	0,69	0,53	0,56
Average Isc [mA]	0,69	0,56	0,57
R [A/W]	0,461	0,375	0,377
EQE [-]	0,900	0,731	0,736
SR [A/W]	0,461	0,314	0,266

9.9. Figure: Table with measured and calculated data for monocrystalline silicon solar cells

For the nanoampere method the same technique of evaluation of the data was used. For each wavelength the external quantum efficiency and the spectral responsivity was calculated. We can see that for Si-m cells only the at the highest value 635,2 nanometers of measured wavelength fits to the reference data [1]. At the other two wavelengths of 532 and 447,9 nanometers respectively we can observe that the values are lower then those in the reference responsivity. On the other hand, the shape of the measured curve would be similar if more data was collected.

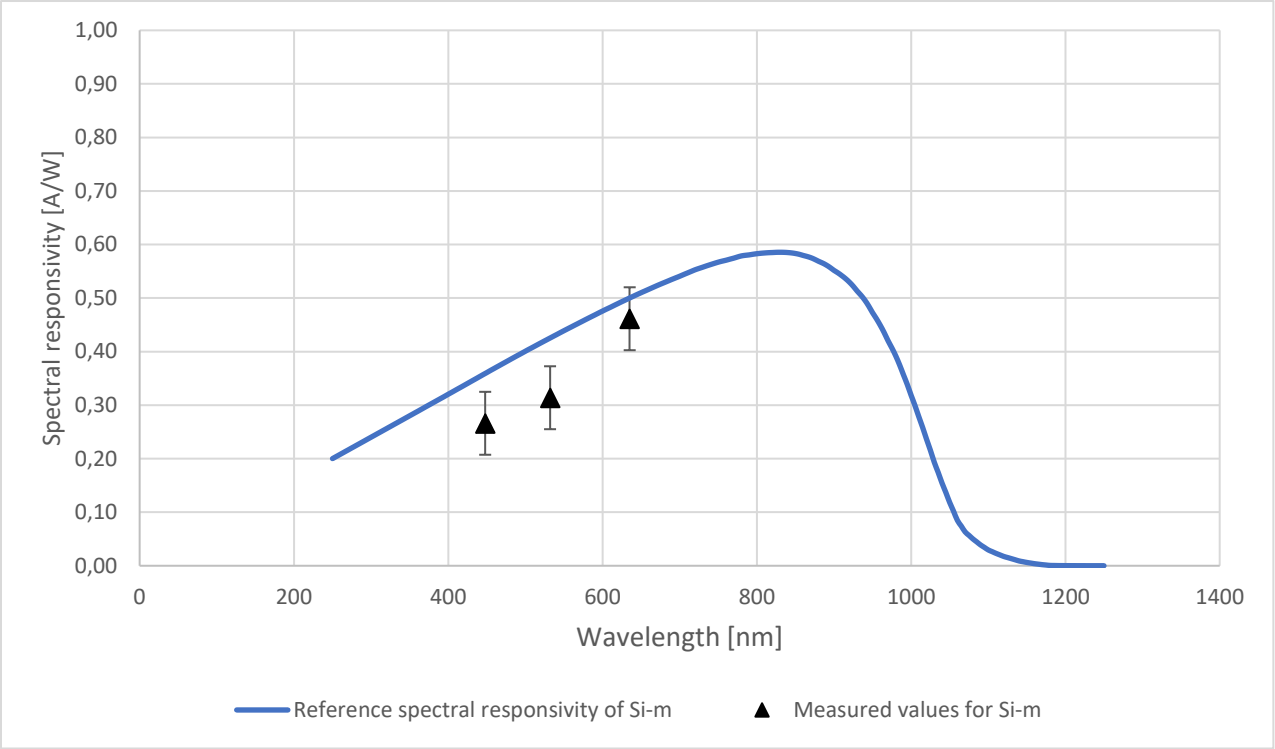

9.10. Figure: Comparing measured and reference data for Si-m cells with nano-ampere method

First, we suspected that these lower measured values may have been caused by the connection cables to this module. During the experiment the cables were changed out to see if this had any effect on them and the difference was negligible. In further experiments however the cables were changed out to shorter ones but from the same type, to minimize the effect they can have on these values.

Decrease of the SR compared to the reference curve in these Si-m cells may have been also caused by the not so consistent bias background light as well. We observed that by changing the direction of the bias light just slightly had a big effect on the measured values. The light scattered in a different pattern at the surface of the module which can have this effect causing measurements errors with very low values of current as in this case. At this point the decision was made to fix the whole set-up as much as possible to eliminate the errors coming from this source.

Other measurements error may have been caused by the characteristic of the measurement itself. The modules homogeneity with respect to SR and light induced current is not even, especially on the edges of the module. As in chapter 10. is shown the lower values at the edge have had a big impact on the average values of light induced current and, in the end, also on SR values.

9.3. Polycrystalline silicon – Nano-ampere method

Measurement no.	I [mA] - R (635,2 nm)	I [mA] - G (532 nm)	I [mA] - B (447,9 nm)
1	0,66	0,59	0,54
2	0,67	0,58	0,53
3	0,68	0,57	0,52
4	0,70	0,59	0,52
5	0,68	0,57	0,51
Average Isc [mA]	0,68	0,58	0,52
R [A/W]	0,452	0,387	0,349
EQE [-]	0,882	0,754	0,681
SR [A/W]	0,452	0,324	0,246

9.11. Figure: Table with measured and calculated data for polycrystalline silicon solar cells

With polycrystalline Si cells the measured data showed that it corresponds and fits to the reference data well. We can see a trend of increasing responsivity with higher wavelengths measured as expected. The first two wavelengths of 447,9 and 532 nanometers show slightly lower values than the reference curve but these values are also within the margin of error.

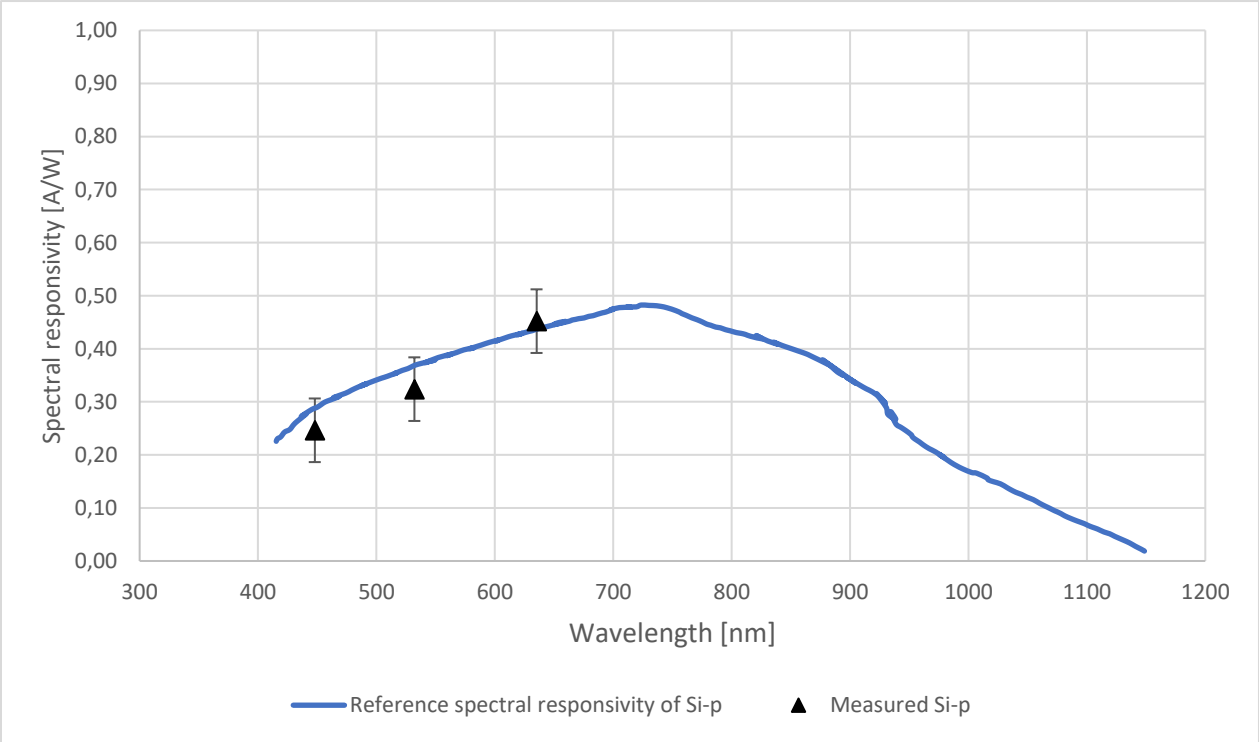

9.12. Figure: Comparing measured and reference data for Si-p cells with nano-ampere method

9.4. Amorphous silicon – Nano-ampere method

Measurement no.	I [mA] - R (635,2 nm)	I [mA] - G (532 nm)	I [mA] - B (447,9 nm)
1	0,30	0,44	0,19
2	0,29	0,45	0,17
3	0,27	0,42	0,18
4	0,28	0,43	0,22
5	0,28	0,41	0,21
Average Isc [mA]	**0,28**	**0,43**	**0,19**
R [A/W]	0,189	0,287	0,129
EQE [-]	0,369	0,559	0,252
SR [A/W]	0,187	0,240	0,091

9.13. Figure: Table with measured and calculated data for amorphous silicon solar cells

For a-Si cells its visible that the largest deviation between the measured and the reference data was present at 447,9 nanometers of wavelength near the blue band. With higher values of wavelength, the data showed to be fit with reference spectral responsivity values. With a-Si cells a lower responsivity was expected from the cells as it was discussed in part 9.1.3.

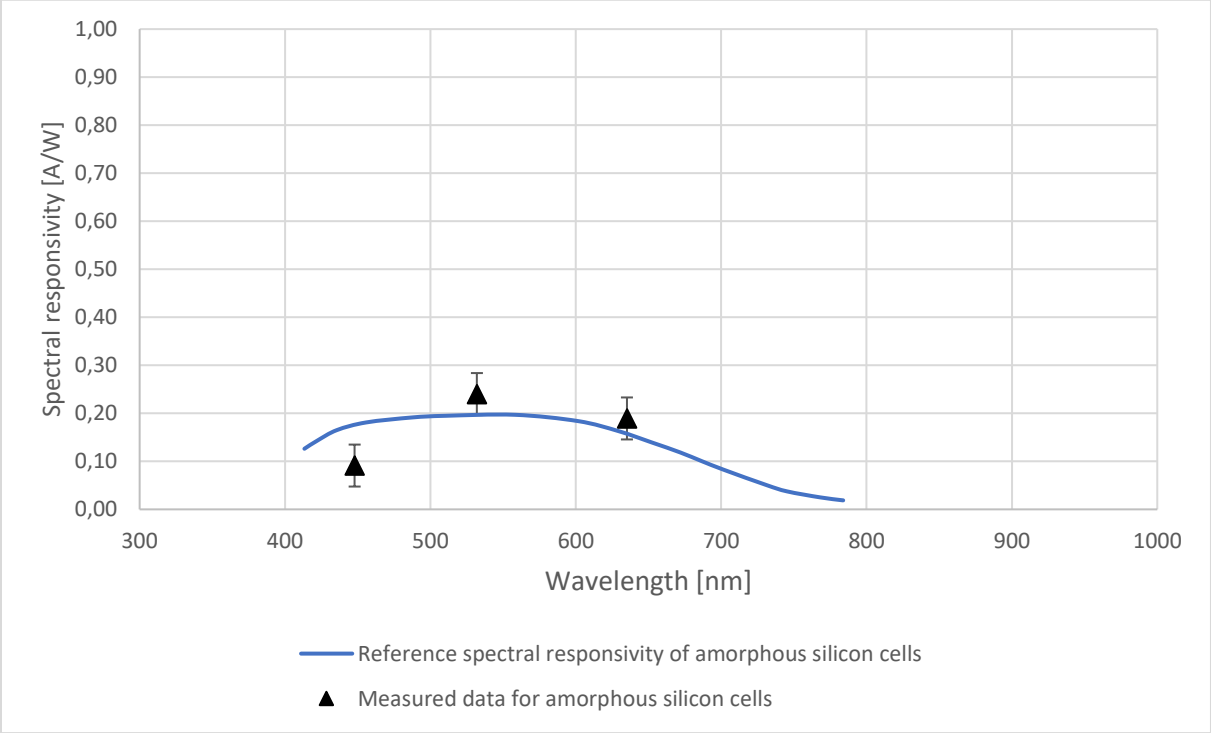

9.14. Figure: Comparing measured and reference data for amorphous Si cells with nano-ampere method

9.5. Perovskite solar cells – Nano-ampere method

Measurement no.	I [mA] - R (635,2 nm)	I [mA] - G (532 nm)	I [mA] - B (447,9 nm)
1	0,57	0,55	0,40
2	0,58	0,55	0,42
3	0,56	0,54	0,41
4	0,57	0,53	0,44
5	0,56	0,54	0,42
Average Isc [mA]	**0,57**	**0,54**	**0,42**
R [A/W]	0,379	0,361	0,279
EQE [-]	0,739	0,705	0,544
SR [A/W]	0,375	0,303	0,196

9.15. Figure: Table with measured and calculated data for perovskite solar cells

Perovskite cells showed very similar results to those ones in the lock-in amplifier method. Average values of short circuit current and the later calculated SR and EQE values fit the data from the reference SR measurements of this type except for the highest wavelength of 635,2 nm near the red band. This might have been caused by the imprecise measurement of the reference power of this red laser, which was redone for this method and gave slightly different values.

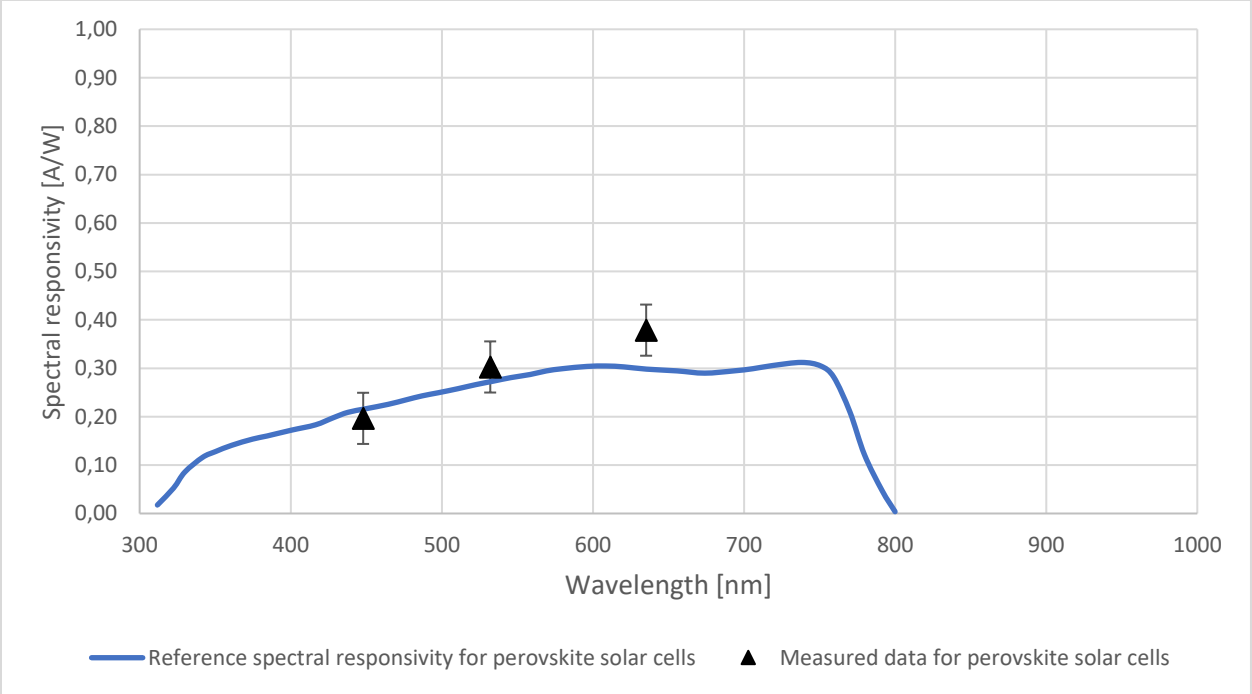

9.16. Figure: Comparing measured and reference data for perovskite cells with nano-ampere method

10. COMPARISON OF MEASUREMENT METHODS

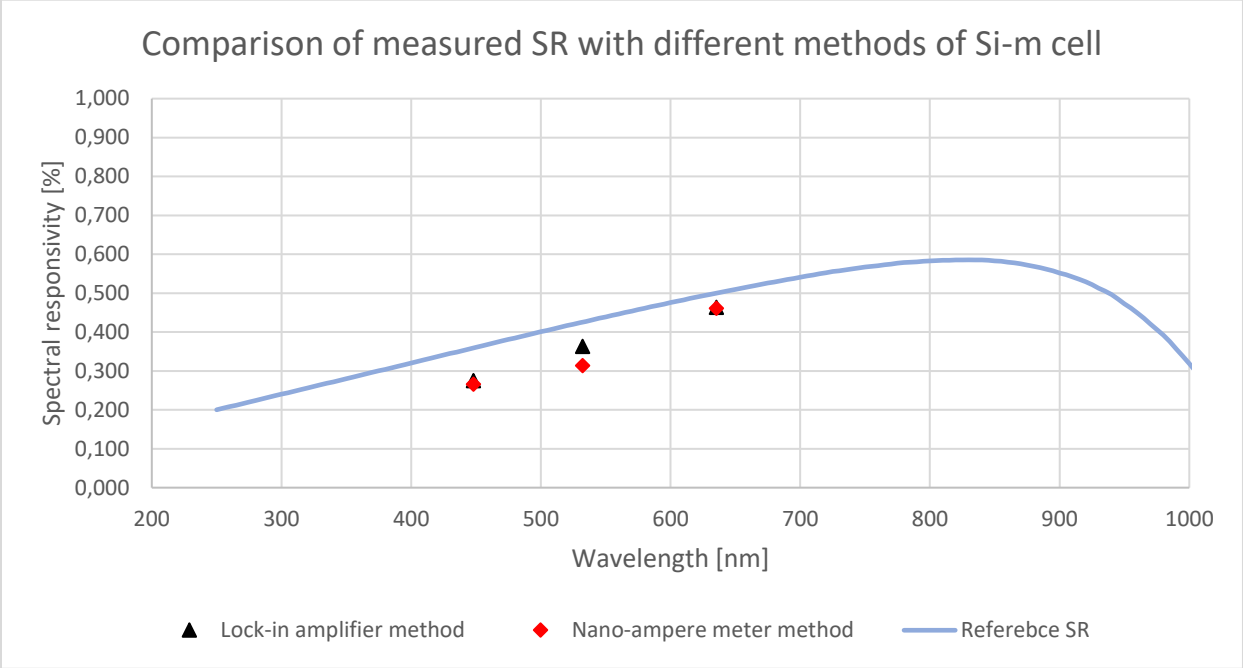

10.1. Figure: Comparison of measured SR data with two different methods for different λ for Si-m cells

As we can see from figure 10.1. there is a slight difference between the values of SR at 532 nm.

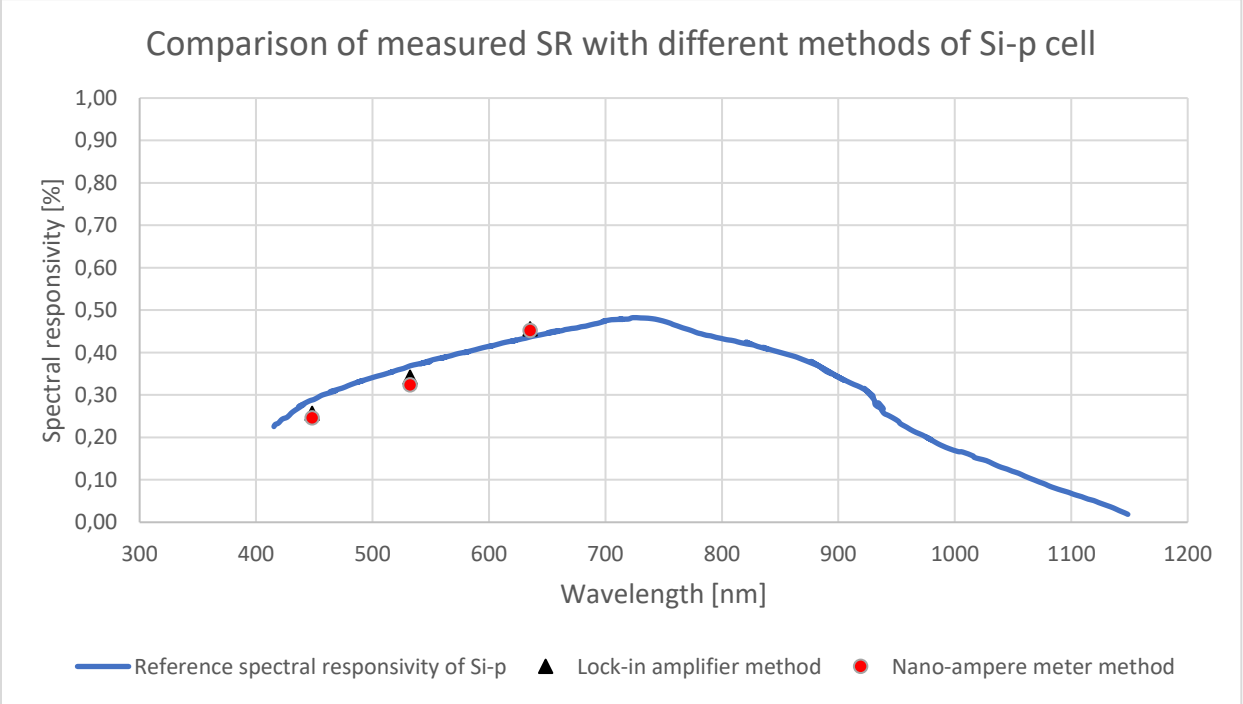

10.2. Figure: Comparison of measured SR data with two different methods for different λ for Si-p cells

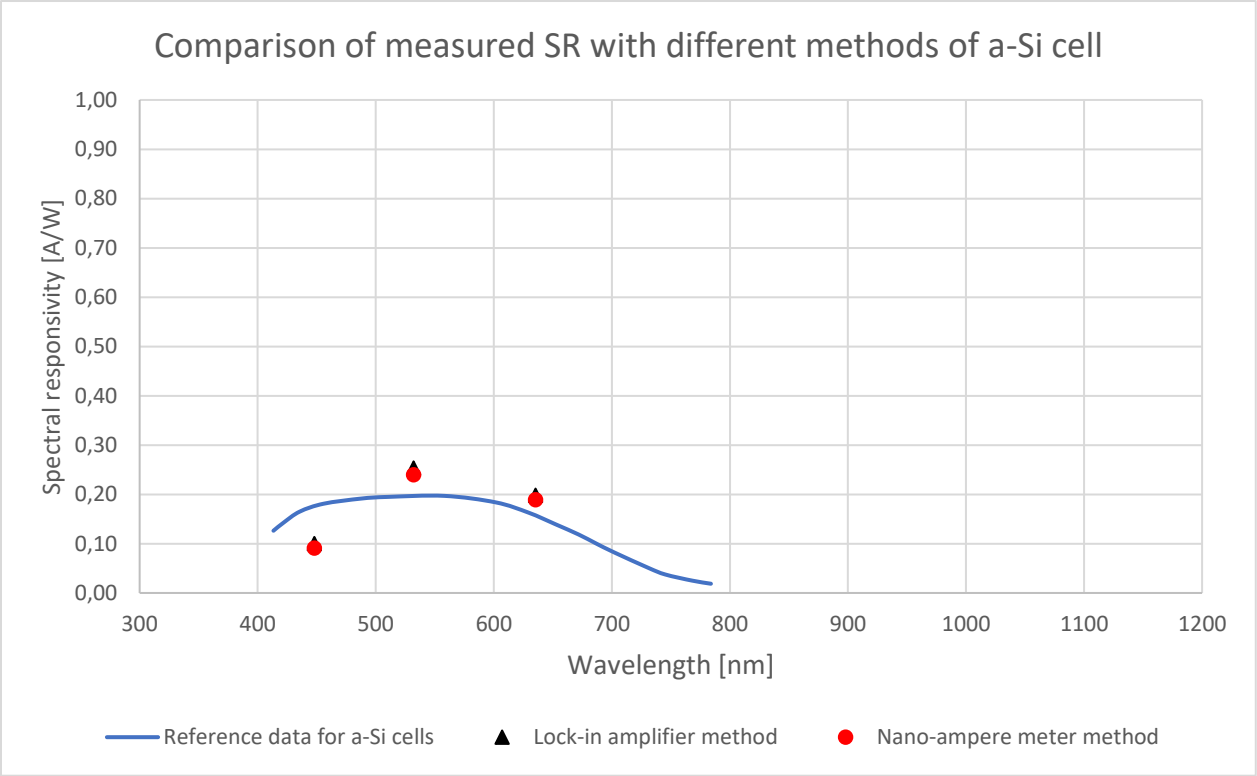

10.3. Figure: Comparison of measured SR data with two different methods for different λ for a-Si cells

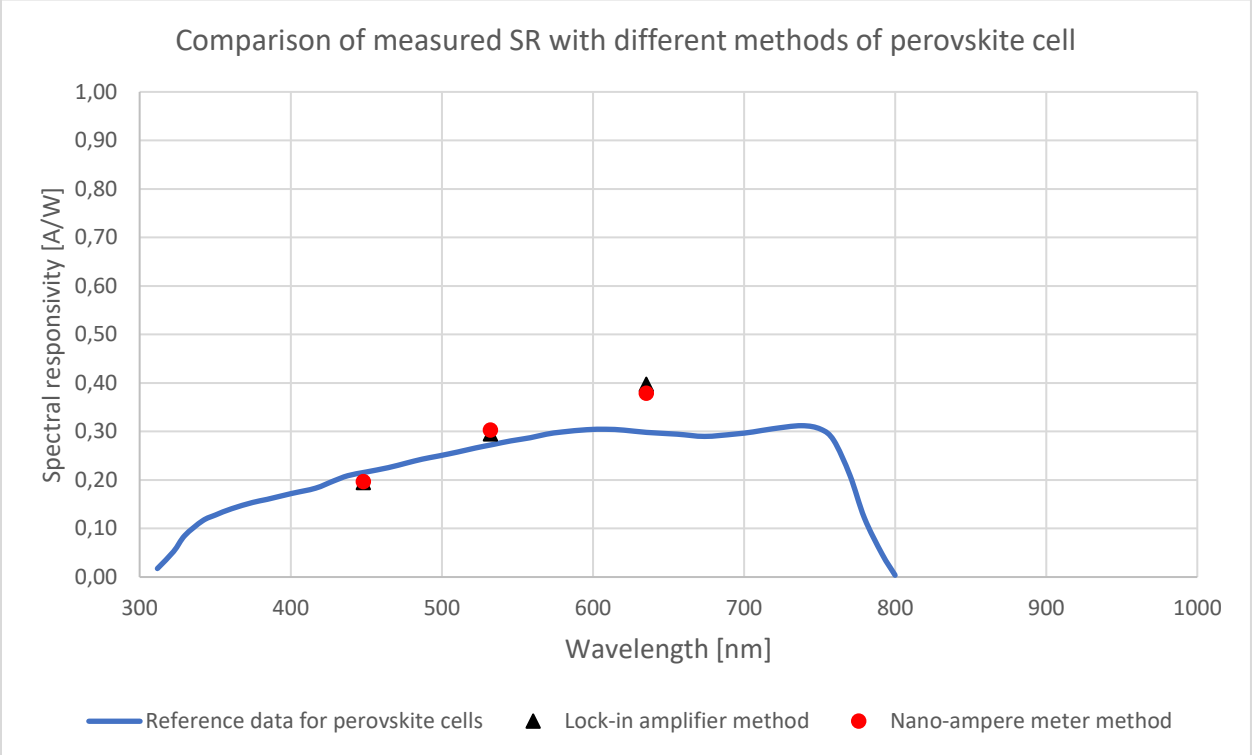

10.4. Figure: Comparison of measured SR data with two different methods for different λ for perovskite cell

From these comparisons we can observe that a slight difference is present between the values of the two measuring methods. In the case of Si-m cells for the green band a larger difference is seen, this might have been cause by wrong positioning of the laser itself during the interchange of the two methods.

Nevertheless, the data shows both cases are following the reference curve of the SR for each type of cell. This is good news from the perspective of evaluation because it shows the consistency of the data. The nano-ampere meter method was introduced to get more precise data from the cell itself. Due to the fact that short-circuit current values can be very small this could be an important step to eliminate as much errors as possible.

For further improvement the use of a more precise bias background light would be appropriate.

In the next table the comparison between the methods is shown based on absolute percentual differences:

Wavelength [nm]	**447,9 nm**	**532 nm**	**635,2 nm**
Si-m	3,39 %	15,59 %	0,55 %
Si-p	4,20 %	5,52 %	0,88 %
a-Si	1,31 %	5,58 %	4,93 %
Perovskite	-0,96 %	-2,58 %	4,93 %

10.5. Figure: Table with comparison of method data in absolute percentual figures

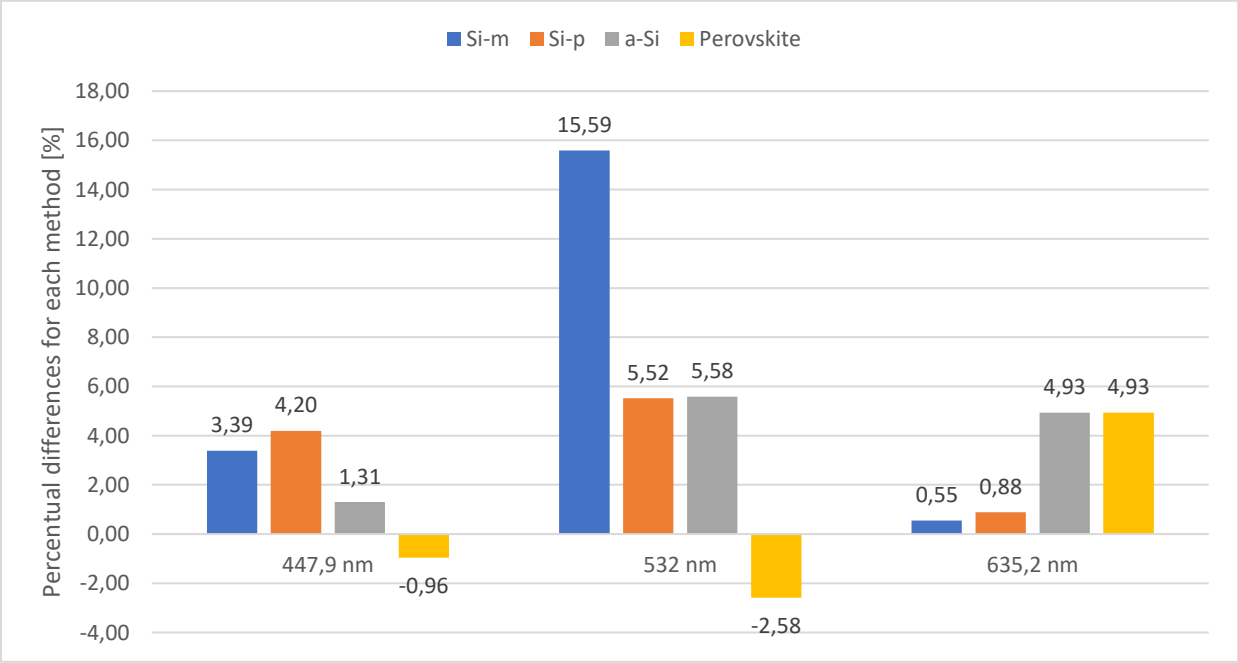

10.6. Figure: Comparison of method data in percentual figures

11. HOMOGENEITY OF SPECTRAL RESPONSE

We wanted to also evaluate the homogeneity of the spectral response of the modules. This was possible in two cases for the Si-m and the Si-p modules. The measurement was done by dividing the modules into 9x9 zones based on the number of the cells present in the module itself. For each zone the laser beam was shined to the geometrical middle of each cell. For these purposes 5 measurements were done for each cell for a total number of measurements of 810. These values were later evaluated in Excel. In the following graphs the homogeneity of the induced current is shown in relative to the maximal values of achieved currents from the cell.

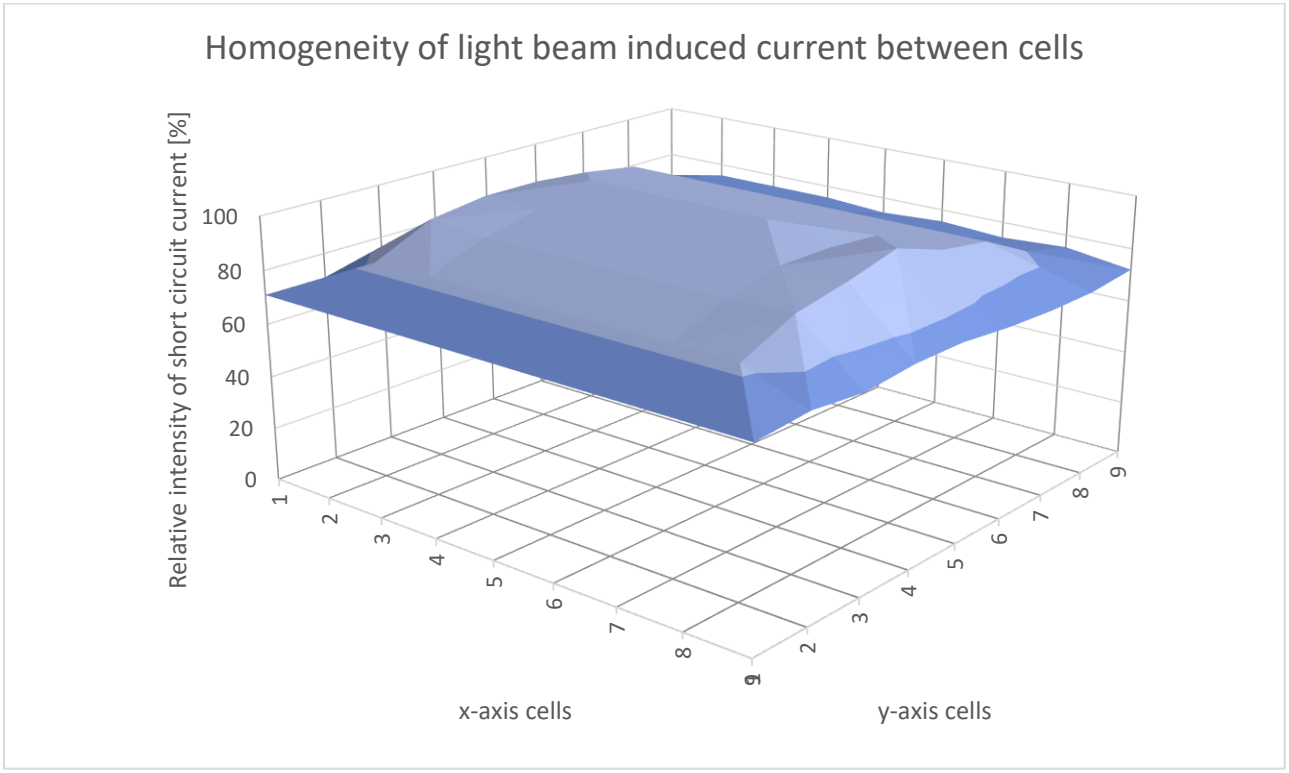

11.1. Figure: Homogeneity of light beam induced current between individual cells for Si-m

As we can see for the Si-m cells the homogeneity of the light induced current is well distributed in middle section of the zones. Here the values of current were 80% or above respective to the maximal achieved measured short-circuit currents. In the zones at the edge of the module we can observe slightly lower values of current reaching from 80 to 70% in some cases. This decrease was observed in each of the measurements. It is well known behavior of these types of modules that the cells at the edge are less likely to perform as good as those in the middle. This is caused partly by the structural and electrical parameters regarding resistivity of the module itself.

On the next graph we can see the same evaluation for the Si-p module. The data shows that relative intensity of light beam induced current was lower in these compared to those in the Si-m. Zones in the middle part of the module show lower percentage of maximal values at around 80% or even lower. The cells in the edge of the module showed even lower intensity with around 70% and lower values.

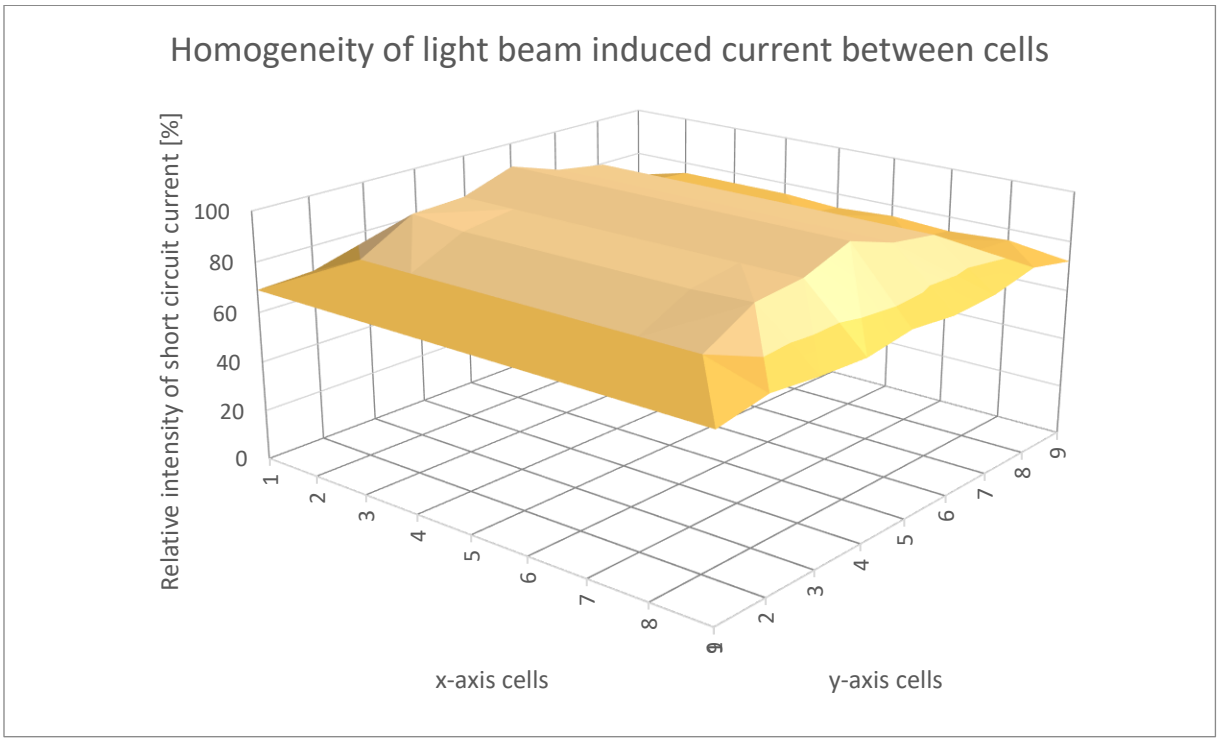

11.2. Figure: Homogeneity of light beam induced current between individual cells for Si-p

These measured currents are an average response from all three wavelengths. Their individual percentual values are represented in the next graph for Si-m cells.

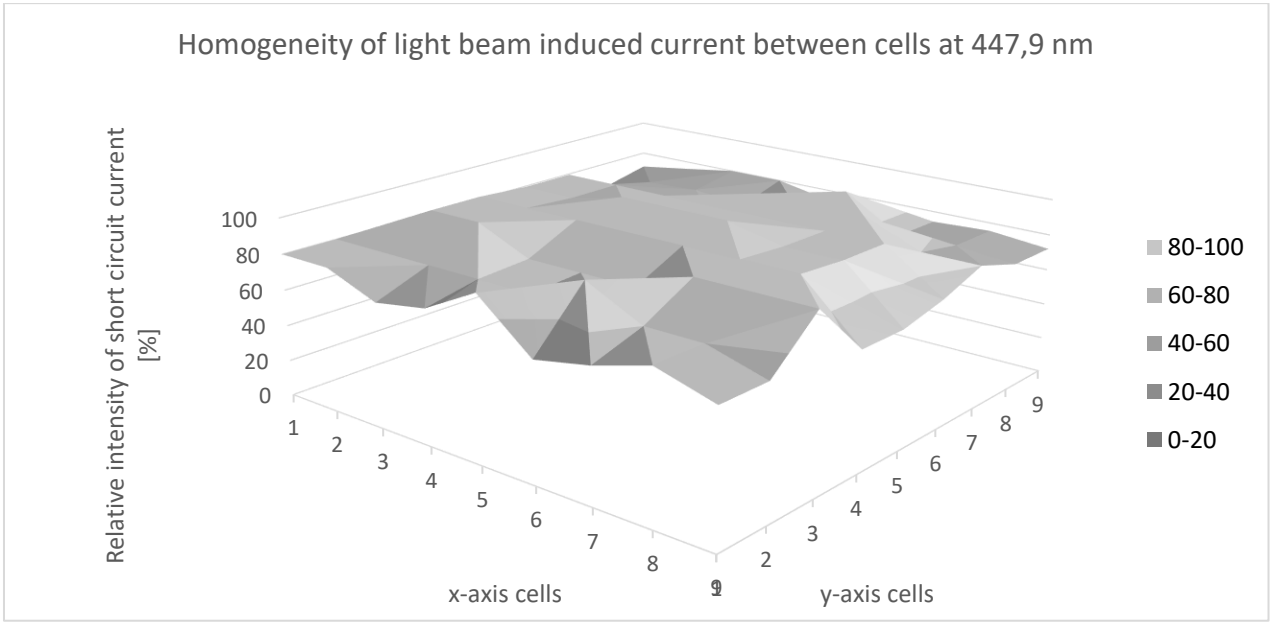

11.3. Figure: Homogeneity of light beam induced current at 447,9 nm for Si-m cells

In the following graphs we can see the relative intensity of light induced current for each wavelength measured. In these cases the Si-m module is shown only as the data for Si-p cells were very similar and are included in the previous part discussing homogeneity.

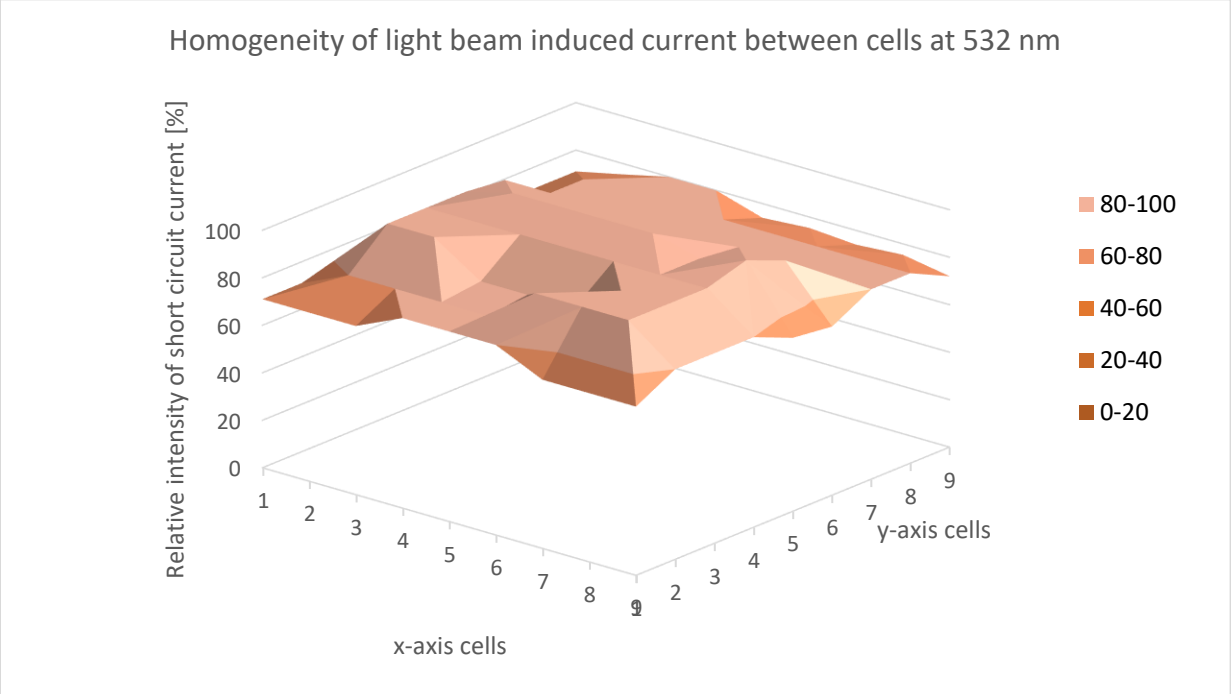

11.4. Figure: Homogeneity of light beam induced current at 532 nm for Si-m cells

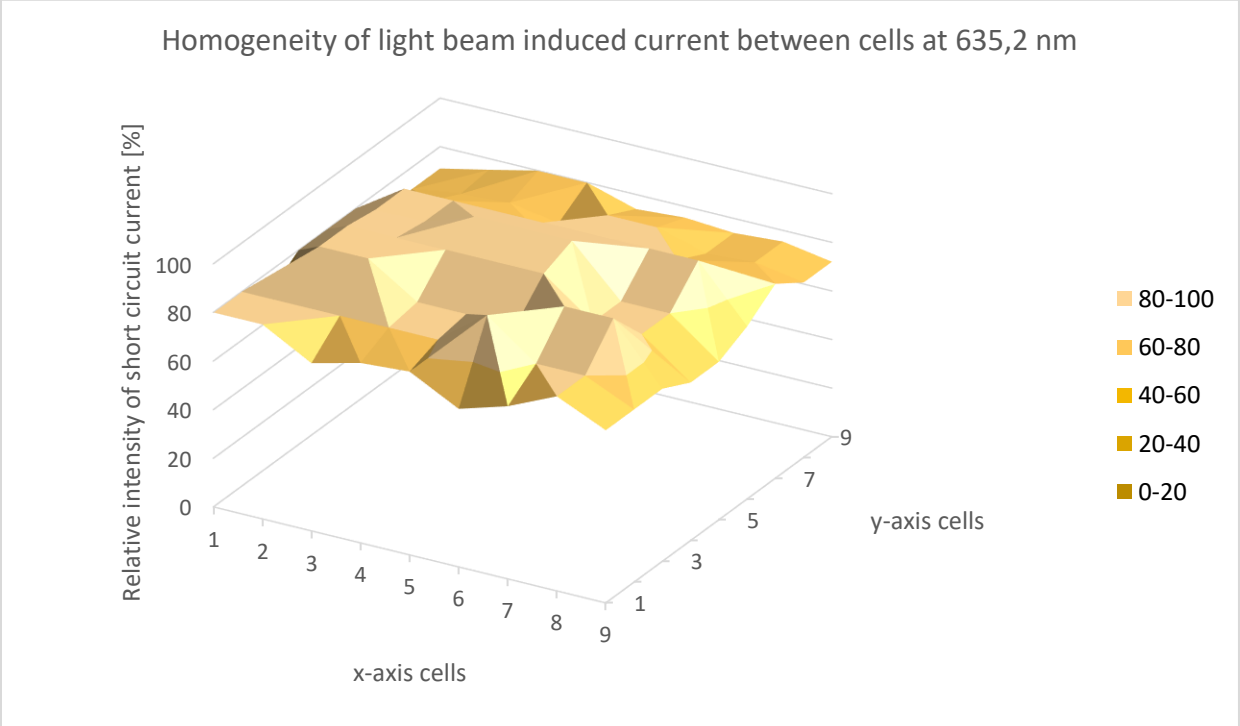

11.5. Figure: Homogeneity of light beam induced current at 635,2 nm for Si-m cells

11.1. Evaluation of homogeneity

With the homogeneity shown in the three graphs we can see that the main tendency of decreased values at the edges of the module are present at every wavelength tested. This brings the question what is causing these decreased values on average.

One of the possible reasons of the non-uniform cell response might be microcracking or metallization defects which can reduce power output. These defects are not easily identifiable but with measuring different parts of the modules response we can show where exactly are these non-uniformities.

The short circuit current can be very sensitive to the distance between the light beam and the contact on the grid, due to this its mainly dependent on the series resistance value. As mentioned for the microscopic ruptures in the material itself we can show by common LBIC methods that these ruptures can act as short circuit. This can end in the reduction of the shunt resistance value therefore influencing possibly the short circuit current measurements.

This evaluation can also show the non-homogeneity or homogeneity of the doping materials of the cell.

From previous studies [28] we know that the cell itself inside has different distribution of SR and light beam induced current values. Near the edges of the cell there can be a reduced current response. The side of the cell which doesn't have the interconnections attached to the metallization can show a better response. This effect might be caused by the process used in attaching these interconnections and with it damaging the edges of the cell. Under this process heat and pressure is present which can cause severe defects in the material under certain circumstances.

Overall, these effects within the cell can show up also while measuring the whole module for the homogeneity. During the measurements it wasn't possible to place the laser beam in the same position for every single cell. This might have caused that for different cells we got slightly different results of SR and current as the characteristics of the cells in the measured part differed.

12. RESPONSIVITY OF A CELL WITHIN A MODULE

In this part we will examine the possibility of measuring the SR from a cell within the module itself. We decided to use the same technique shown in the previous chapters. This means a laser beam is pointed at different points of the cell itself. Each measurement was done 5 times for these points and overall 5 times for each wavelength totaling in 25 measurements/wavelength. We measured the light induced current from the cell using a lock-in amplifier which filters out the background bias light necessary for the whole module to work.

12.1. Measured data

For the measurement a cell from the middle zone of the 9x9 module was selected. This was partly based on the data from our previous experiments of homogeneity where these cells gave the highest currents during our measurements.

Measurment no.	I [nA] - R (635,2 nm)	I [nA] - G (532 nm)	I [nA] - B (447,9 nm)
1	0,077	0,068	0,062
2	0,065	0,064	0,063
3	0,078	0,061	0,064
4	0,074	0,060	0,062
5	0,077	0,059	0,062
Avarage I [nA]	0,07	0,06	0,06
R [A/W]	0,494	0,416	0,419
EQE [-]	0,964	0,812	0,818
SR [A/W]	0,494	0,349	0,296

12.1. Figure: Measured values of SR for Si-m cell

Measurment no.	I [nA] - R (635,2 nm)	I [nA] - G (532 nm)	I [nA] - B (447,9 nm)
1	0,060	0,054	0,049
2	0,061	0,053	0,048
3	0,062	0,052	0,047
4	0,064	0,054	0,047
5	0,062	0,052	0,046
Avarage I [nA]	0,06	0,05	0,05
R [A/W]	0,411	0,352	0,318
EQE [-]	0,802	0,686	0,619
SR [A/W]	0,411	0,294	0,224

12.2. Figure: Measured values of SR for Si-p cell

12.2. Evaluation of measured data

For our evaluation of the data, we plotted the measured SR together with the data from the previous chapter with average SR for the whole module. Values are divided based on the used wavelengths of the laser beams.

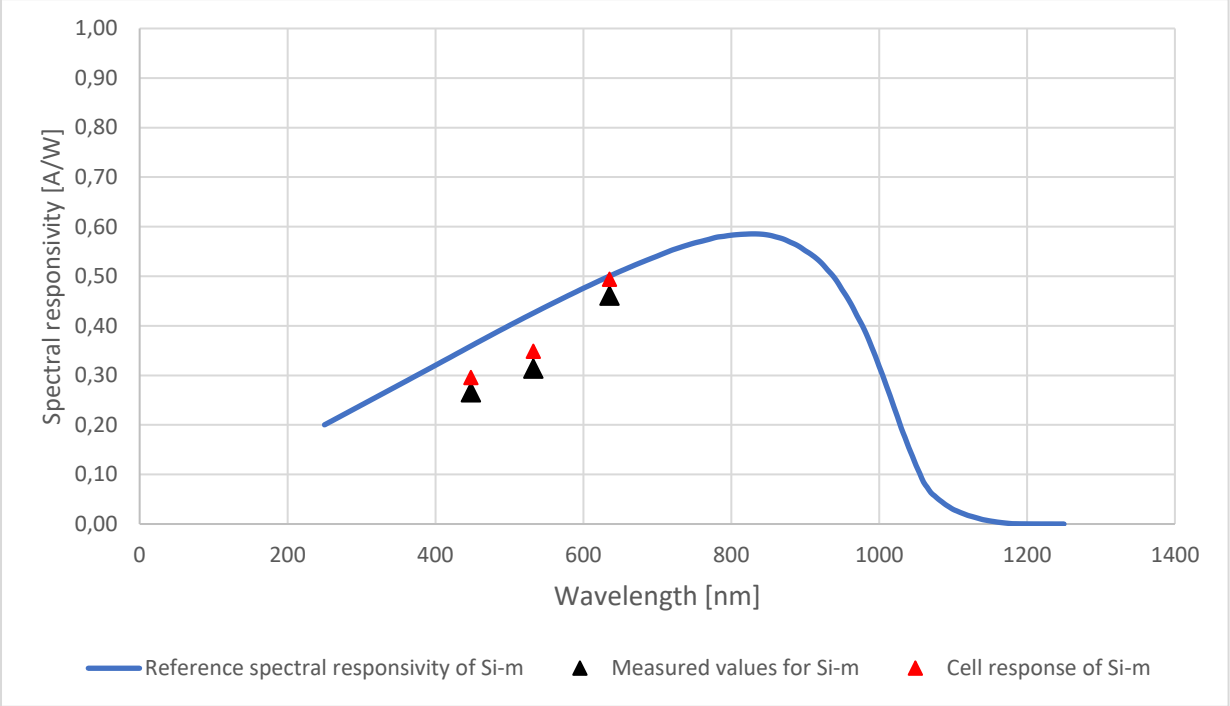

12.3. Figure: Comparing SR cell response to reference and whole module values for Si-m

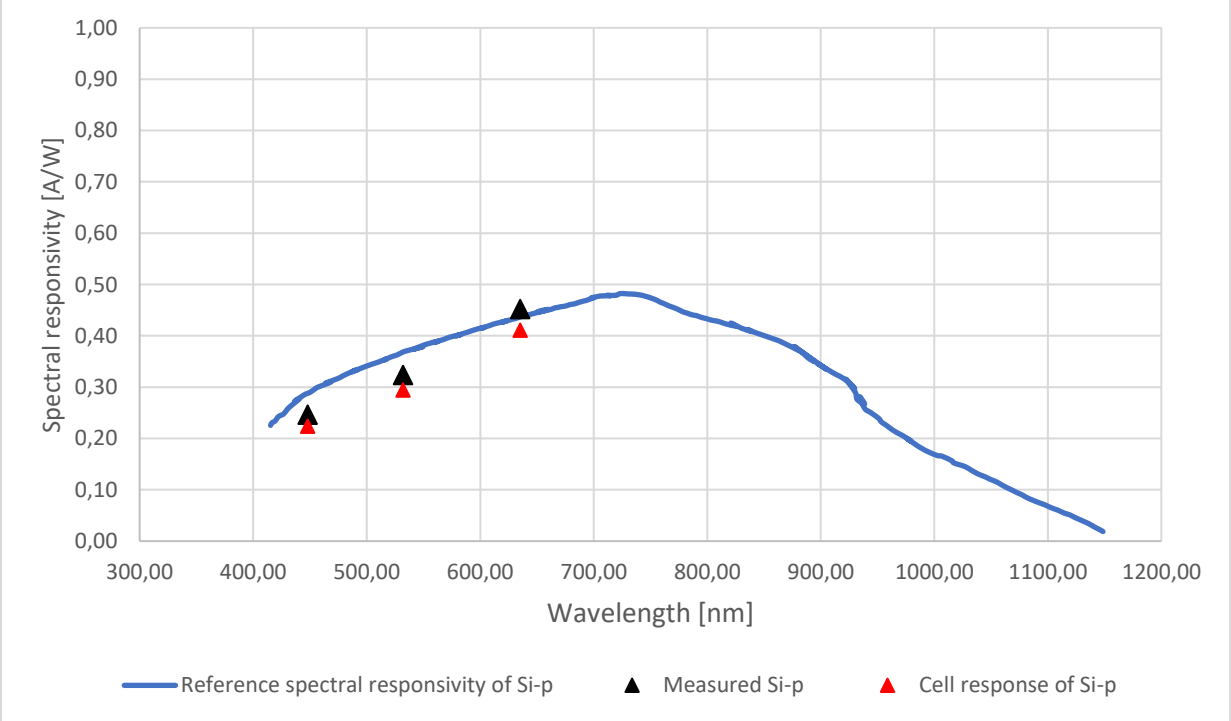

12.4. Figure: Comparing SR cell response to reference and whole module values for Si-p

From the figures 12.3 and 12.4 respectively we can observe that for the Si-m cells the response was slightly higher compared to the data what we got for the whole module. On the other hand, in this case this was closer to the reference curve of SR for Si-m cells. These higher values could've been caused by the fact that for the whole module we consider every. Those ones on the edge are less efficient in converting light to current as it was discussed in the previous chapter. These lower values had an impact on the average as a whole for the module.

With the data for the Si-p cell there was a tendency for this particular cell to give lower values of currents and SR as those average ones. For the purpose of comparing these responses we intended to keep the same cell choice for both modules.

This method can be used also to investigate and explain the differences in manufacturing processes and its variations. For example, higher temperature stress can induce changes in the material itself which can have the effect of decreasing the efficiency of the cells. These defective cells with damaged areas often show larger variations in the data of uniformity.

13. COMPARING SR TO AM1.5 REFERENCE SPECTRA AND ITS CONVERSION

One of the goals of this work was to compare the measured data of spectral responsivity to the AM1.5 reference spectrum.

13.1. Figure: Comparison of SR with AM1.5 for Si-m cells

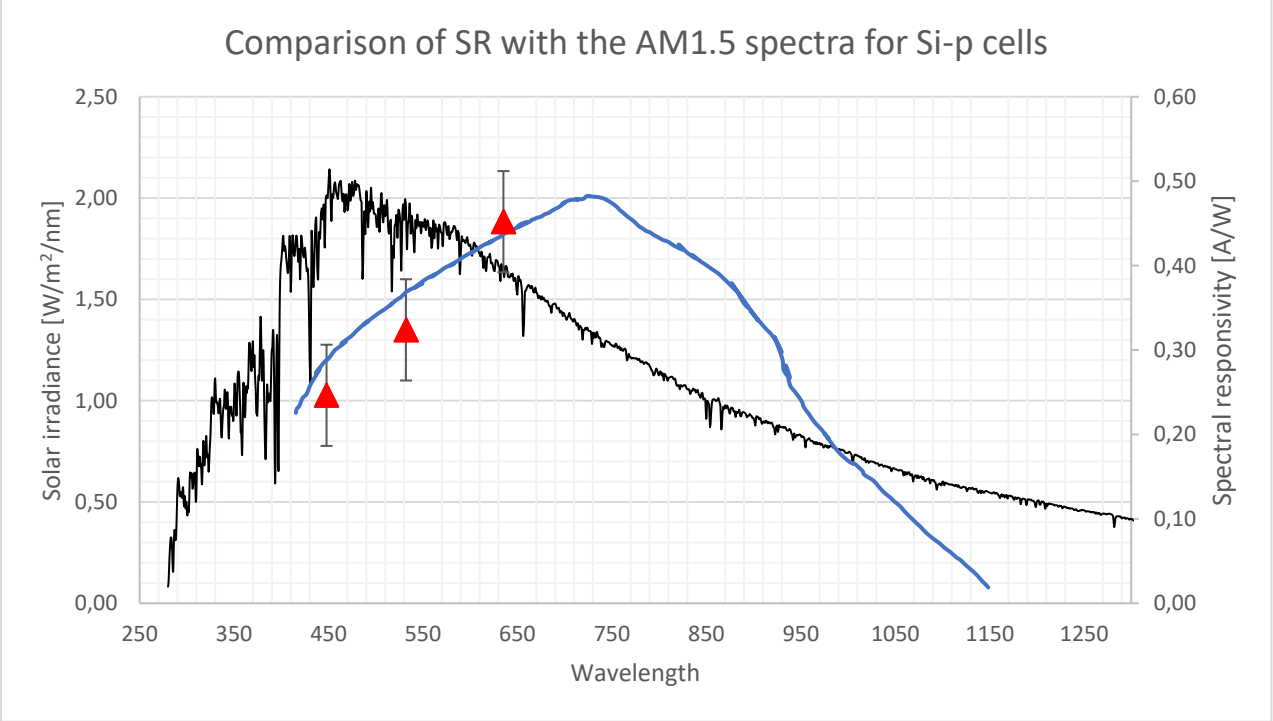

13.2. Figure: Comparison of SR with AM1.5 for Si-p cells

As we can see in plots 13.1. and 13.2. the reference spectral response doesn't show sharp spectroscopic features as the irradiance spectra of AM1.5. From the plot we can also see the band at which these cells can be the most effective in converting light to electrical current. These values with the AM1.5 can be used to determine the spectral mismatch factor M by integrating the short-circuit current values. In our measurements however this wasn't possible because of the lack of data for other wavelengths of the spectra. For further experiments of this type a higher resolution of the wavelength would be suggested. On the other hand we can see that even with these measured values we can get a good look into at what parameters of solar light these cells are operating optimally.

If the measurements were done with a step size of at least 5 nm we would get acceptable data for the spectra which is not as sharp as the AM1.5. This would allow us to create the irradiance product of AM1.5 and the SR, because the data points for the EQE and SR respectively would have very similar resolution of the irradiance data of Am1.5.

As it was shown in other studies [29] using key values of irradiance $E\ (\lambda)$ we can calculate and determine the spectral mismatch factor M. For this we need four inputs: the solar reference spectrum, the irradiance of a bias light spectrum, the reference SR of a cell and the cell we intend to test. First, we need to measure the SR of the reference cell and also calculate the integral of the short-circuit currents. Later we determine the product of $E_{AM1.5}\ (\lambda)$ and $SR_{ref}\ (\lambda)$. We also measure as previously mentioned the $E_b\ (\lambda)$ of the bias light itself and the $SR_{cell}\ (\lambda)$ of the cell tested. From these datapoints and by the equation following:

$$M = \frac{\int_{\lambda_1}^{\lambda_2} E_{AM1.5}\ (\lambda)\ SR_{ref}\ (\lambda)\ d\lambda}{\int_{\lambda_1}^{\lambda_2} E_b\ (\lambda)\ SR_{ref}\ (\lambda)\ d\lambda} \cdot \frac{\int_{\lambda_1}^{\lambda_2} E_b\ (\lambda)\ SR_{cell}\ (\lambda)\ d\lambda}{\int_{\lambda_1}^{\lambda_2} E_{AM1.5}\ (\lambda)\ SR_{cell}\ (\lambda)\ d\lambda} \qquad (8)$$

The spectral mismatch factor can be used as a correction factor to adjust for the current density measured for a specific test device. [29]

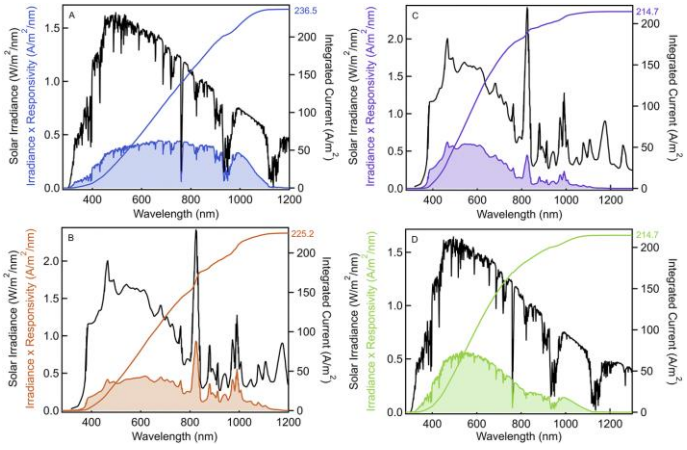

13.3. Figure: Plot of the four key irradiance E(λ) values and the product with spectral responsivity [29]

These measurements can help us more accurately achieve device optimization with minimizing errors. Also, it can provide more precise data on efficiencies of solar cells in general, which is a very important aspect nowadays.

14. SUMMARY

One of the main goals of this thesis was to measure the spectral responsivity of different types of photovoltaic modules and cells, evaluate the quality of the used method and to give a perspective on materials still in the early stages of development like perovskites. In this work it was shown that the homogeneity of the modules differs vastly between each cell. These studies further confirm the need of new approaches regarding the possibility of increasing the efficiency. It is important to accurately characterize the effectiveness of each cell within a module as it can get us more data on the larger scale behavior. Spectral response measurement allows to characterize these cells in a way which incorporates all technical aspects, mainly mechanical and electrical. These testing capabilities allow multi-junction cell manufacturers to optimize their process and produce greater cells with higher efficiencies. LBIC in general is a reliable tool for cell and module evaluation as it can show a wide aspect of non-uniformities. As these methods develop in the future LBIC can become more practical with improvements in lasers and the data-evaluation.

This work also showed us that these methods can be also combined with other investigation techniques. For example, the possibility to study the same cells and areas at different laboratories it can be beneficial for the scientific community as well as for the industry itself.

By introducing more precise measuring methods for example by increasing the sampling resolution based on the wavelength in the future it's possible to use this easy and simple method to determine PV cell performance and compare the data to reference values.

Another significant part of this work discussed the examination of new technologies in the PV industry with hands-on experiments. Perovskites have the potential to bring increased efficiency values for a much cheaper production price. As we saw from the data the characteristics of these cells can be very similar to those ones used today by the industry.

In the future these measuring methods can provide the PV manufacturers of new solar cell types like perovskite good data on their cell's performance. As we are headed for a future, where the use of energy and the consumption of natural resources are key factors of our destiny it is becoming a more significant part of our lives to implement new and more efficient technologies.

LIST OF FIGURES

REFERENCES

[1] "PVEducation." https://www.pveducation.org/ (accessed Feb. 04, 2021).

[2] P. J. Mohr, B. N. Taylor, and D. B. Newell, "CODATA recommended values of the fundamental physical constants: 2006," *Rev. Mod. Phys.*, vol. 80, no. 2, pp. 633–730, Jun. 2008, doi: 10.1103/RevModPhys.80.633.

[3] G. Laufer, *Introduction to Optics and Lasers in Engineering*, 1st ed. Cambridge University Press, 1996. doi: 10.1017/CBO9781139174190.

[4] "Light," *Wikipedia*. Dec. 31, 2020. Accessed: Feb. 04, 2021. [Online]. Available: https://en.wikipedia.org/w/index.php?title=Light&oldid=997375394

[5] D. J. Griffiths, *Introduction to electrodynamics*, 3. ed., Reprinted with corrections. Upper Saddle River, NJ: Prentice Hall, 1999.

[6] "Photoelectric effect," *Wikipedia*. Aug. 11, 2021. Accessed: Aug. 12, 2021. [Online]. Available: https://en.wikipedia.org/w/index.php?title=Photoelectric_effect&oldid=1038240801

[7] A. T. Fromhold, *Quantum mechanics for applied physics and engineering*, Repr. New York: Dover, 1991.

[8] G. D. Mahan, "Theory of Photoemission in Simple Metals," *Phys. Rev. B*, vol. 2, no. 11, pp. 4334–4350, 0 1970, doi: 10.1103/PhysRevB.2.4334.

[9] C. Mee, *International A/AS level physics*. London: Hodder Education, 2008.

[10] "Reference Air Mass 1.5 Spectra." https://www.nrel.gov/grid/solar-resource/spectra-am1.5.html (accessed Aug. 12, 2021).

[11] "Fig. 3. Solar spectral irradiance at air mass 1.5 (AM 1.5) collected...," *ResearchGate*. https://www.researchgate.net/figure/Solar-spectral-irradiance-at-air-mass-15-AM-15-collected-from-American-Society-for_fig1_311445954 (accessed Jun. 16, 2021).

[12] "Solar Spectra." https://www.nrel.gov/grid/solar-resource/spectra.html (accessed Aug. 12, 2021).

[13] C. Riordan and R. Hulstron, "What is an air mass 1.5 spectrum? (solar cell performance calculations)," in *IEEE Conference on Photovoltaic Specialists*, Kissimmee, FL, USA, 1990, pp. 1085–1088. doi: 10.1109/PVSC.1990.111784.

[14] "Light Beam Induced Current (LBIC) - Freiberg Instruments - lifetime, single crystal orientation, PID, automation and more." https://www.freiberginstruments.com/upcdmdp/applications/light-beam-induced-current-lbic.html (accessed Aug. 12, 2021).

[15] "Different Types of Solar Cell," *The Renewable Energy Hub*. https://www.renewableenergyhub.co.uk/main/solar-panels/types-of-solar-cell/ (accessed Aug. 06, 2021).

[16] "Amorphous silicon," *Wikipedia*. May 06, 2021. Accessed: Aug. 07, 2021. [Online]. Available: https://en.wikipedia.org/w/index.php?title=Amorphous_silicon&oldid=1021694197

[17] "Polycrystalline silicon," *Wikipedia*. Jun. 07, 2021. Accessed: Aug. 07, 2021. [Online]. Available: https://en.wikipedia.org/w/index.php?title=Polycrystalline_silicon&oldid=1027431706

[18] "Figure 3: Amorphous silicon solar cell device structure [9]," *ResearchGate*. https://www.researchgate.net/figure/Amorphous-silicon-solar-cell-device-structure-9_fig1_276205737 (accessed Aug. 06, 2021).

[19] "Czerny-turner.png (600×372)." https://upload.wikimedia.org/wikipedia/commons/e/e8/Czerny-turner.png (accessed Feb. 04, 2021).

[20] "Tunable Lasers Revisited | Light Reading." https://www.lightreading.com/ethernet-ip/tunable-lasers-revisited/d/d-id/587547 (accessed Feb. 04, 2021).

[21] "SuperK EXTREME supercontinuum lasers - NKT Photonics," *LASERS & FIBERS*. https://www.nktphotonics.com/lasers-fibers/product/superk-extreme-fianium-supercontinuum-lasers/ (accessed Feb. 04, 2021).

[22] "SuperK VARIA tunable filter - NKT Photonics," *LASERS & FIBERS*. https://www.nktphotonics.com/lasers-fibers/product/superk-varia-tunable-single-line-filter/ (accessed Feb. 04, 2021).

[23] “Semilab | Products.” https://semilab.com/category/products/light-beam-induced-current (accessed Aug. 07, 2021).
[24] “RS PRO | RS PRO 5W Polycrystalline solar panel | 904-6128 | RS Components.” https://int.rsdelivers.com/product/rs-pro/stp005rsbp/rs-pro-5w-polycrystalline-solar-panel/9046128 (accessed Aug. 12, 2021).
[25] “Polycrystalline Solar Panel EX-150P-36 150W 12V.” https://merkasol.com/Polycrystalline-Solar-Panel-EX-150P-36-150W-12V (accessed Aug. 12, 2021).
[26] A. Pourakbar Saffar and B. Deldadeh Barani, “Thermal effects investigation on electrical properties of silicon solar cells treated by laser irradiation,” *IJRED*, vol. 3, no. 3, pp. 184–187, Oct. 2014, doi: 10.14710/ijred.3.3.184-187.
[27] H. Wei *et al.*, “Flash-evaporation printing methodology for perovskite thin films,” *NPG Asia Mater*, vol. 9, no. 6, pp. e395–e395, Jun. 2017, doi: 10.1038/am.2017.91.
[28] A. Ibrahim, “LBIC Measurements Scan as a Diagnostic Tool for Silicon Solar Cell,” p. 7, 2011.
[29] M. O. Reese, A. R. Marshall, and G. Rumbles, “CHAPTER 1 Reliably Measuring the Performance of Emerging Photovoltaic Solar Cells,” pp. 1–32, 2017, doi: 10.1039/9781782626749-00001.